NTNU – Trondheim
Norwegian University of
Science and Technology

Modelling and Analysis of a Cylindrical Flare Tower

Kjetil Legard

Marine Technology
Submission date: June 2013
Supervisor: Bernt Johan Leira, IMT

Norwegian University of Science and Technology
Department of Marine Technology

NTNU
Norwegian University of Science and Technology
Department of Marine Technology

Master thesis, Spring 2013
for
Stud. Techn. Kjetil Legard

Design of a Novel Cylindrical Flare Tower

Design av et Nytt Sylindrisk Flammetårns-konsept

Design of a novel structural concept for a flare tower located on an offshore platform is to be addressed in the present Master thesis. Representation of the static and dynamic loads on such a tower will also need careful consideration due to the novelty of the structural layout. Based on information received from 5D Group, the candidate shall perform an initial modeling and assessment of the structure. Hand calculations can be applied at an early stage of the analysis.

Subsequently, more detailed numerical response analyses are to be performed by means of the computer program ANSYS, which is able to represent nonlinear structural behavior. The following types of design criteria are to be addressed: Ultimate Limit State (ULS, also including buckling analysis), Fatigue Limit State (FLS, also including VIV analysis) and Accidental Limit State (ALS).

The following subjects are to be addressed as part of this work:

1. Give a general description of typical designs of existing flare towers and the loads that need to be taken into account. Discuss which design guidelines that are relevant for these types of structures. Describe the DNV and NORSOK rules for such structures in more detail.

2. Establish a model of the structure that is suitable for analysis by the Finite Element Computer Program ANSYS. A brief description of the theoretical background for the algorithms which are implemented in this program is to be given. Convergence studies are to be performed in relation to relevant static load patterns in order to ascertain that the applied mesh has an adequate refinement.

3. Design analyses of the flare tower with respect to the limit states mentioned above are to be performed (i.e. the ULS, FLS and ALS). Inertia forces due to the dynamic motion of the supporting platform structure are to be included. Random dynamic response analyses are to be performed by application of the established Finite Element model in ANSYS.

4. Optimization of the structural characteristics in terms of the longitudinal and ring stiffener system is to be performed to the extent that time allows. Alternative geometrical layouts of the ventilation cut-outs including their shape and position characteristics are also to be considered. Minimization of stress concentrations around these cut-outs is to be elaborated upon.

The work-scope may prove to be larger than initially anticipated. Subject to approval from the supervisor, topics may be deleted from the list above or reduced in extent.

In the thesis the candidate shall present his personal contribution to the resolution of problems within the scope of the thesis work. Theories and conclusions should be based on mathematical derivations and/or logic reasoning identifying the various steps in the deduction. The candidate should utilise the existing possibilities for obtaining relevant literature.

The thesis should be organised in a rational manner to give a clear exposition of results, assessments, and conclusions. The text should be brief and to the point, with a clear language. Telegraphic language should be avoided.

The thesis shall contain the following elements: A text defining the scope, preface, list of contents, summary, main body of thesis, conclusions with recommendations for further work, list of symbols and acronyms, references and (optional) appendices. All figures, tables and equations shall be numerated.

The supervisor may require that the candidate, at an early stage of the work, presents a written plan for the completion of the work. The plan should include a budget for the use of computer and laboratory resources which will be charged to the department. Overruns shall be reported to the supervisor.

The original contribution of the candidate and material taken from other sources shall be clearly defined. Work from other sources shall be properly referenced using an acknowledged referencing system.

The thesis shall be submitted in 3 copies:

- Signed by the candidate
- The text defining the scope included
- In bound volume(s)
- Drawings and/or computer prints which cannot be bound should be organised in a separate folder.

Supervisor: Professor Bernt J. Leira Contact person at 5D Group: Arild Hobæk

Start: January 14th, 2013 Deadline: June 24th, 2013

Trondheim, January 14th 2013

Bernt J. Leira

Preface

This is a master thesis at Institute of Marine Technology, NTNU. The assignment was provided by Arild Hobæk at 5D Group AS, who also have been of great assistance with ANSYS modelling and general guidance. Professor Bernt J. Leira has been the supervisor for the project. He has defined the assignment and been of great help throughout the semester.

I would also like to thank fellow students at office A2.003, for participating in general unwinding by the means of table tennis sessions.

Scope

As proposed by 5D Group AS, a novel flare tower design has been investigated. A general description of existing flare towers and the new concept are to be presented. The governing guidelines forms the baseline for the design, with NORSOK and DNV guidelines as the primary framework. A model suitable for finite element analysis is to be generated. Quasi-static and dynamic analysis are to be performed, in accordance to the given design codes. The flare tower may prove to need strengthening in terms of stiffening with both longitudinal and ring stiffeners. Buckling have to be considered as a potential collapse mechanism, with shell imperfections and cut-outs. The lifetime of the flare tower is to be determined utilizing a fatigue analysis, including the contributions from vortex-induced vibrations.

Summary

The study of a cylindrical flare tower concept proves that this novel flare tower design has great potential and could be a competetor to traditional truss-work flare towers. A design capable of withstanding wind and sea loads are developed.

A conical model was developed for finite element analysis, with decreasing diameter from process deck to the top of the flare tower. The tower was split into three sections, as the wind moment would give larger stresses at the bottom of the tower, than of those at the top. The total height of the tower is 70 meters with a bottom diameter of 5 meters. The diameter at the free end is 3 meters. The tower is a steel structure with different shell thickness for each section. To avoid buckling collapse, longitudinal stiffeners are present at the bottom section, while ringstiffeners are included at the bottom and mid section. Cut-outs are also present to minimize the wind loads by ventilation. The loads have been calculated using the Frøya wind model and Frøya wind spectrum, providing wind loads for quasi-static and dynamic analysis, respectively. Accelerations from platform movements were provided from 5D Group AS and included in the analyzes. All finite element analyzes, performed in ANSYS, revealed stresses well within the acceptable range. The dynamic response amplitudes were low. However, some stress concentrations were found around the cut-outs from the quasi-static analysis. The buckling capacity of the shell structure was determined by a non-linear buckling analysis, with maximum fabrication tolerances included as the material imperfections. Vortex-induced vibrations were investigated, giving small cross-flow and in-line amplitudes. Using the hot spot stress from ANSYS, a fatigue analysis was performed to determine the lifetime of the flare tower. The fatigue analysis shows no initiation of fatigue cracks under the given environmental loads. Since the stress concentrations did not prove to initiate fatigue crack during the given lifetime, this proves that the flare tower is slightly oversized.

Sammendrag

Studiet av et nytt sylindrisk flammetårn viser at det nye flammetårndesignet har stort potensial og kan være en konkurrent til de tradisjonelle flammetårn av fagverkskonstruksjoner. Studien viser at denne type design kan motstå store vind og havlaster.

En konisk modell ble generert for elementmetode-analyse, med avtagende diameter fra prosessdekket til toppen av tårnet. Modellen ble delt inn i tre seksjoner, siden momentet fra vinden ville gi de største påkjenninger i bunnen av tårnet. Flammetårnets totale høyde er 70 meter med en diameter på 5 meter i bunn. I toppen er diameteren 3 meter. Tårnet er av stål og de tre seksjonene har forskjellig skalltykkelse. Langsgående stivere er inkludert på den nederste seksjonen og ringstivere brukt på den nederste og midterste seksjonen. Utkapp er også modellert for å minke vindlaster ved ventilasjon. Belastningene er beregnet ved hjelp av Frøya-vindmodellen og Frøya-spekteret, og gir vindlaster for kvasi-statisk og dynamisk analyse. Akselerasjoner fra plattformbevegelser ble tildelt fra 5D Group AS og er inkludert i analysene. Alle elementmetode-analyser, utført i ANSYS, viste spenninger godt innenfor det akseptable området. De dynamiske responsamplitudene var små. Imidlertid ble noen spenningskonsentrasjoner funnet rundt utkappene fra kvasi-statisk analyse. Knekkspenningen av skallstrukturen ble utregnet ved en ikke-lineær knekkingsanalyse, med maksimale fabrikasjontoleranser som materialimperfeksjoner. VIV ble undersøkt og ga små tverrstrøms- og medstrømsamplituder. Spenningskonsentrasjonene fra ANSYS, ble brukt i en utmattingsanalyse utført for å bestemme levetiden til flammetårnet. Utmattingsanalysen viser ingen tegn til tretthetsbrudd under gitte miljøbelastninger. De høye spenningskonsentrasjonene har ført til at strukturen er noe overdimensjonert, da det viste seg at de ikke ville gi noe tretthetsbrudd innenfor den angitte levetiden.

Contents

List of Figures

List of Tables

Symbols and Abbreviations

Symbols

f_y - Yield strength
γ_m - Material factor
U_0 - Mean wind speed 10 meters above sea level
u(z,t) - Design wind speed
U(z) - Mean wind speed
C - Wind coefficient
I_u - Turbulence intensity
q - Wind pressure
Δf - Frequency increment
F_w - Wind force
Δ - Roughness parameter
$g_{so,h}$ - Gravity component from pitch motions
η_{5a} - Pitch amplitude
M_x - Torsional moment
A_m - Enveloping area
t - Shell thickness
τ - Shear stress
τ_{max} - Maximum shear stress
f_s - Shear capacity
L - Section length
r - Section radius
A_{req} - Required ring stiffener area
Z_l - Curvature parameter
s - Stiffener spacing
f_E - Elastic buckling strength
C - Buckling coefficient
H - Web height
B - Flange width
t_w - Web thickness

t_f - Flange thickness
e_f - Flange eccentricity
ω_n - Eigenfrequency
$\overline{\omega}_n$ - Eigenvalue
f - Frequency
t_e - Effective shell thickness
A - Stiffener area
S(f) - Spectral density
$\widetilde{f}$ - Spectrum frequency
$S_w(f)$ - Wind pressure spectrum
$\overline{q}$ - Mean wind pressure
$\overline{u}$ - Mean wind speed
C - Damping
λ - Damping ratio
β,α - Damping coefficient
δ - Material imperfections
g - length of circular template
σ - Tangential stress
K_c - Keulegan-Carpenter number
T - Wind period
U - Wind speed
C_A - Added mass coefficient
C_{DS} - Drag coefficient for steady flow
m_e - Equivalent mass
m_a - Added mass
K_s - Stability parameter
δ - Logarithmic decrement
ζ - Damping ratio
St - Strouhal number
f_s - Vortex shedding frequency
Re - Reynolds number
V_R - Reduced velocity
A_{CF} - Cross-flow amplitude
γ - Mode shape parameter
y_{max} - Maximum deflection from mode shape
y(x) - Mode shape
N - Number of cycles to failure
n - number of cycles
$\overline{a}$,m - S-N parameter
$\Delta\sigma$ - Stress range
$f(\Delta\sigma)$ - Two-parameter Weibull distribution

h,q - Weibull parameter
$Q(\Delta\sigma)$ - Exceedance probability
D - Accumulated fatigue damage

Abbreviations

DNV - Det Norske Veritas
ULS - Ultimate limit state
ALS - Accidental limit state
UF - Utilization factor
VIV - Vortex-induced vibrations
DFF - Design fatigue factor
FEM - Finite element method
FEA - Finite element analysis

Constants

$g = 9.81 m/s^2$ - Gravity acceleration
$\rho_a = 1.226 kg/m^3$ - Air density
$\rho_s = 7850 kg/m^3$ - Steel density
$C_s = 0.65$ - Constant shape coefficient
$E = 2.1 \cdot 10^5 MPa$ - Young's modulus
$\upsilon = 0.3$ - Poisson's ratio
$\gamma_m = 1.15$ - Material factor
n = 0.468 - Frøya spectrum constant

Chapter 1

General Description

1.1 Flare Towers

Flare towers, or flare stacks, are found on both industrial plants and on oil production sites. In industrial plants flare towers serve their main purpose by burning of flammable gas released from pressure relief valves. On offshore oil productions sites the flare towers are primarily used for burning of natural gas, which is associated with the production of oil. This is mainly performed at offshore oil rigs or platforms which do not have any connection with gas piping or infrastructure for transportation of gas. The flare is often elevated so that it is not a hazard to personnel and process on the onshore or offshore installation.

1.2 Typical Design

Existing flare towers are mainly designed as standard truss work and is used as supporting structure for the flare pipe. One of the main advantages with this type of structure is the small amount of material required to obtain sufficient capacity. This gives a low weight compared to the overall strength of the structure.

However, the production of such structures has proven to be demanding and expensive. There are a large amount of joints and as the truss work flare tower are of great dimensions, the process of welding becomes time consuming. The welded joints will also be more exposed to fatigue since the stresses tend to concentrate at these points.

1.3 Cylindrical Concept

A cylindrical concept for a flare tower is to be investigated. If such a design will prove to have sufficient strength capacity it would have several advantages. The construction of the cylindrical flare tower would be less complex, giving reduced cost due to less production time. An optimization of the flare tower can give reduced weight and shield the flare pipe against wind loads. In addition, the stresses will be less concentrated around certain points such as welded joints, giving a structure less exposed to fatigue.

However, this type of design will be far more vulnerable to wind loads with a larger area which will be subjected to wind. The wind speeds at the top of the flare tower will be of great magnitude on an offshore location, giving large stresses near the bottom of the tower due to the moment. The focus in this assignment will be as low weight as possible and reduced production costs, but the eigenfrequency and dynamic response of the flare tower will also be of great concern. This will be discussed further throughout the thesis.

1.4 Relevant Guidelines

There are a large amount of guidelines relevant for the flare tower as it is part of an offshore structure. In this assignment the DNV guidelines will be applicable, with emphasis on DNV-OS-C101 Design of Offshore Steel Structures as design basis. The environmental loads are in accordance with DNV-RP-C205 Environmental Conditions and Environmental Loads. As the tower needs to be resistant against buckling, DNV-RP-C202 Buckling of Shells be the governing guideline for this design check. The mentioned guidelines contains references to other guidelines such as NORSOK N-003, NORSOK N-004, the Eurocode guidelines and many others. These guidelines will be described in more detail and further discussed throughout the assignment.

Chapter 2

Loads

2.1 Description

Flare towers on offshore structures are often exposed to a harsh environment. The North Sea environment will be the focus in this assignment.

As the cylindrical flare tower has a large area compared to conventional designs, this will result in a structure more exposed to wind loads. The wind loads will be divided into static and dynamic loads, containing a mean wind speed and a fluctuation component. For objects exposed to a time varying wind load a detailed dynamic wind analysis should be performed [1], which represents the wind fluctuations. The flare tower is assumed to be welded to the process deck of a floating unit, such as FPSO or semi-submersible. This will give a contribution from the sea environment to the inertia loads due to movements.

2.2 Design Wind Speed

For wind calculations the Frøya wind profile was chosen, as proposed for offshore wind locations [1]. This wind profile includes the wind fluctuations and serves as a quasi-static wind model and a good approximation to the dynamic contributions. The Frøya wind profile uses the one hour mean wind speed 10 meters above sea level, U_0, as main parameter. This parameter is provided from table 2.1 , which is the extreme value of the mean wind speed. The 100-year value is chosen for the design basis.

Measured wind data forms the basis, which is collected in the interval 1973 to 2002, at the locations Statfjord, Brent, Stevenson, Troll and Gullfaks C. These datas are provided from the Statoil Metocean Report [10] and are highly representative for the North Sea environment.

The wind speeds are presented below with corresponding return period.

Return Period [years]	**1 hour**	**10 min**	**1 min**
1	32.0	35.4	39.7
10	36.0	40.0	45.2
100	40.0	44.8	51.0
10000	46.0	52.0	59.8

Table 2.1: Extreme wind speed

For strong wind conditions the design wind speed at height z above sea level is given by

$$U(z,t) = U(z) \cdot \left[1 - 0.41 \cdot I_u \cdot \ln\left(\frac{z}{10}\right)\right] \tag{2.1}$$

where the 1-hour mean wind speed is given by

$$U(z) = U_0 \cdot \left[1 + C \cdot \ln\left(\frac{t}{t_0}\right)\right] \tag{2.2}$$

where

$$C = 5.73 \cdot 10^{-2} \cdot \sqrt{1 + 0.15 \cdot U_0} \tag{2.3}$$

and the turbulence intensity $I_u(z)$ is given by

$$I_u = 0.06 \cdot [1 + 0.043 \cdot U_0] \cdot \left(\frac{z}{10}\right)^{-0.22} \tag{2.4}$$

In equation 2.1, the variable t is an averaging time period less than or equal to $t_0 = 3600$ s, which corresponds to 1-hour.
The design wind speed is calculated using MATLAB, with an averaging time period of 15 seconds. This is proposed in the Statoil Metocean Report [10], for structures with dimensions exceeding 50 meters in either horizontal or vertical direction. The design wind profile is illustrated in fig. 3.1.

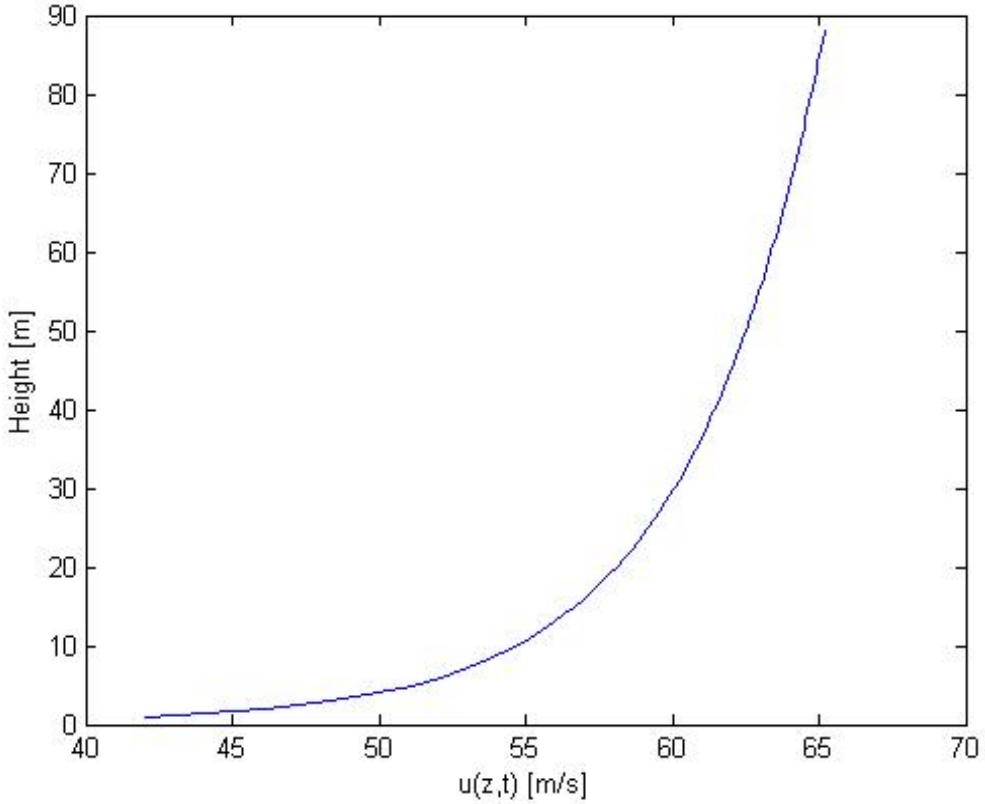

Figure 2.1: Design Wind Profile

Here the wind speed is plotted as a function of height.

2.3 Wind Force

By the proposal from DNV[1, p. 51] it follows that the linearized wind pressure is given by

$$q = \frac{1}{2}\rho_a {U_{T,z}}^2 + \frac{1}{2}\rho_a U_{T,z} u \tag{2.5}$$

where the first term represents the static wind conditions and the second term represents the dynamic wind fluctuations. In the dynamic term, u represents the fluctuating wind speed component as plotted in figure 2.2.

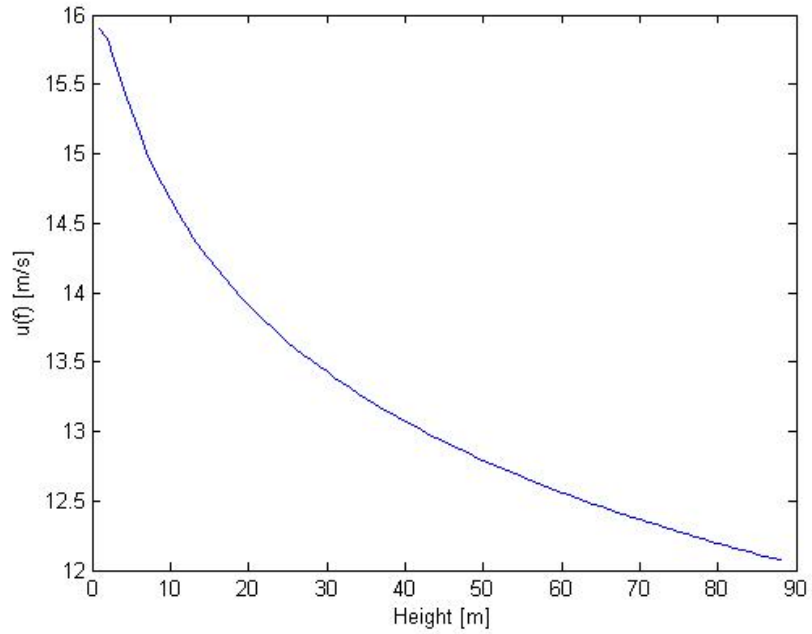

Figure 2.2: Wind Speed Fluctuation Component

The wind force per length unit is given by

$$F_w = C_s D q \sin \alpha \tag{2.6}$$

The roughness of the structure is given by

$$\Delta = \frac{k}{D} \tag{2.7}$$

and assumed less than 10^{-4}, which is smooth, in this case. This results in a constant shape coefficient, C_s, of 0.65 for large Reynolds numbers ($R_e > 10^6$)[1].

2.4 Inertia Forces

2.4.1 Selfweight

Inclination of the tower is an effective way of getting the flare in such distance away from the process deck, that it is not a hazard for production and personnel. The flare tower is inclined with 15 degrees, to avoid adding more

height to the structure. However this results in larger stresses as this will give an increased moment acting on the flare tower.

2.4.2 Accelerations

The flare tower will be designed for offshore locations and exposed to large accelerations due to the sea environment and movement of the rig. Both horizontal and vertical movements will have a large impact on the stresses acting on the structure. The accelerations are provided by 5D Group and represents typical values for a FPSO.

Return Period	**Wave Cond.**		**Loaded Draft**		**Ballast Draft**	
	Hs	**Tp**	**Std. (rms)**	**Max Amp.**	**Std. (rms)**	**Max Amp.**
1-year-Max Hs	10,5	13,5	0,37 m/s^2	1,4 m/s^2	0,49 m/s^2	1,8 m/s^2
10-year-Max Hs	13,1	16,0	0,52 m/s^2	1,9 m/s^2	0,61 m/s^2	2,2 m/s^2
100-years; Min Tp)	15,7	16,0	0,65 m/s^2	2,4 m/s^2	0,75 m/s^2	2,7 m/s^2
100 years; Mean Tp	15,7	17,5	0,61 m/s^2	2,2 m/s^2	0,68 m/s^2	2,5 m/s^2
1000 years; Max Tp	15,7	19,5	0,57 m/s^2	2,1 m/s^2	0,63 m/s^2	2,3 m/s^2

Table 2.2: Vertical accelerations

In the table above the vertical accelerations are represented with maximum expected amplitude and RMS-value over based on a 3 hours duration of sea states.

Return Period	**Wave Condition**		**Loaded Draft**		**Ballast Draft**	
	Hs	**Tp**	**Std. (rms)**	**Max Amp.**	**Std. (rms)**	**Max Amp.**
1-year-Max Hs	10,5	13,5	0,28 m/s^2	1,1 m/s^2	0,31 m/s^2	1,2 m/s^2
10-year-Max Hs	13,1	16,0	0,33 m/s^2	1,2 m/s^2	0,36 m/s^2	1,3 m/s^2
100-years; Min Tp)	15,7	16,0	0,40 m/s^2	1,5 m/s^2	0,44 m/s^2	1,6 m/s^2
100 years; Mean Tp	15,7	17,5	0,38 m/s^2	1,4 m/s^2	0,41 m/s^2	1,5 m/s^2
1000 years; Max Tp	15,7	19,5	0,35 m/s^2	1,3 m/s^2	0,39 m/s^2	1,4 m/s^2

Table 2.3: Horizontal accelerations

To take account for the second order movements the horizontal movements will also have an additional contribution which is the gravity component from the heeling angle [11, p. 153].

In this case this yields

$$g_{so,h} = g \sin(\eta_{5a}) \tag{2.8}$$

where the max expected pitch amplitude is presented in table 2.4.

Return Period	**Wave Cond.**		**Loaded Draft**		**Ballast Draft**	
	Hs	**Tp**	**Std. (rms)**	**Max Amp.**	**Std. (rms)**	**Max Amp.**
1-year-Max Hs	10,5	13,5	0,8 deg	2,9 deg	1,1 deg	4,2 deg
10-year-Max Hs	13,1	16,0	1,1 deg	4,0 deg	1,5 deg	5,3 deg
100-years;Min Tp	15,7	16,0	1,4 deg	5,0 deg	1,8 deg	6,5 deg
100 years; Mean Tp	15,7	17,5	1,3 deg	4,6 deg	1,7 deg	6,0 deg
1000 years; Max Tp	15,7	19,5	1,2 deg	4,2 deg	1,6 deg	5,6 deg

Table 2.4: Wave frequency pitch motions

Chapter 3

Flare Tower Design

3.1 Design Considerations

For design purposes the flare tower is divided into three sections due to the fact that the stresses will be of a much larger magnitude at the lower part of the flare tower than of those at the upper part. Some sections of the flare tower could be strengthened with ring stiffeners and/or longitudinal stiffeners. The diameter of the tower should not only be of such dimension that it gives sufficient strength capacity and space for the flare pipe, but also easy access to flare piping for maintenance and inspection. The flare tower will be designed in such manner that it withstands the stresses that occur in the cylinder, with buckling as a potential collapse mode. In this process, all calculations are performed using spreadsheets for easy change of parameters and to study the relationship between weight and load capacity. As the dimensions are modified, the stresses change. This creates an iterative process to get sufficient capacity with respect to resistance against yield and buckling. To decrease the production costs, the tower is divided into three sections, with different attributes and actions to prevent failure and oversized design. Each section will consist of rolled plates, welded together to construct a full flare tower.

3.2 Material Properties

With reference to NORSOK[8], structural steel of quality DC4 class III was chosen. This implies that there is a low joint complexity of the structure and that the failure of members will be without substantial consequences due to residual strength. As proposed in NORSOK-M120[9] the yield stress will be $\sigma_y = \frac{355}{\gamma_m}$, where γ_m is the material factor given by NORSOK. This gives the

following material properties

Young's Modulus	$2.1 \cdot 10^5$ MPa
Density	7850 kg/m^3
Poisson's ratio	0.3
Yield strength	309 MPa

Table 3.1: Material Properties

3.3 Dimensions

The total height from process deck to top of the flare tower was set to 70 meters, which is not unrealistic with reference to existing flare towers. There is also an air gap of 16 meters, which will give higher wind loads as the wind speed strongly depends on the height. A conical structure was developed, with decreasing diameter from bottom to top. The diameter at the bottom was set to 5 meters and a top diameter of 3 meters proved to be sufficient. The lower section of tower the has a shell thickness of 23 mm and both longitudinal and ring stiffeners. Longitudinal stiffeners are not present in the mid part of the tower, but ring stiffeners are applied. This section has a wall thickness of 10 mm. The top section has no additional stiffening and 8 mm wall thickness. Stiffener spacing and dimensions will be further discussed in the buckling section.

3.4 Longitudinal Stress

As the wind pressure acts on small parts of the circumference along the height of the flare tower, the stresses and the contribution from the wind pressure will be small and neglected in this assignment. This gives no ring stress. The longitudinal stress has its main components from wind moment, self weight and accelerations due to sea loads. As given in DNV-RP-C202, the axial longitudinal membrane stress is sum of the stresses due to uniform axial force and bending. The inclination of the flare tower gives increased stress due to bending, as the inertia forces will have a component perpendicular to the structure and also contribute to axial stress.

The forces acting on the structure is described in chapter 2 and divided in to sectional loads. Each section counts a length of 23.3 meters, which is 1/3 of the height of the rig.

	Lower section	Mid section	Upper section
Max wind force [N/m]	5432	5079	4577
Mass force [N]	1057092	376161	150925
Horizontal force (accel.) [N]	584040	207828	83386
Vertical force (accel.) [N]	290943	207061	83078

Table 3.2: Force

The largest moments will occur if the wind is acting in the direction of the tower inclination, as well as the horizontal accelerations of the tower.

	Lower section	Mid section	Upper section
Max wind moment [Nm]	15963082	7748840	2491797
Vertical moment (accel.) [Nm]	11085719	1313245	698724
Horizontal moment (accel.) [Nm]	18140853	1767534	940432
Selfweight moment [Nm]	8693118	847004	450656

Table 3.3: Moment

	Section 1	Section 2	Section 3
σ_x **[MPa]**	123,5	99,8	69,2

Table 3.4: Longitudinal stress

3.5 Shear Stress

A torsional moment will occur if the wind attacks normal to the direction of the inclination. The horizontal movements of the platform in the same direction can also contribute to a torsional moment. This gives the torsional moment presented in table 3.5.

Equilibrium of moment about an arbitrary point for a closed cross-section gives[16]

$$M_x = \oint qrds = q \oint rds = q \cdot 2A_m \tag{3.1}$$

where

$$A_m = \frac{1}{2} \oint rds \tag{3.2}$$

	Lower section	**Mid section**	**Upper section**
Tors moment [Nm]	34103935	9516374	3432229

Table 3.5: Torional moment

and

$$q = \tau \cdot t \tag{3.3}$$

With a constant thickness over the cross-section the maximum shear stress is given by

$$\tau_{max} = \frac{1}{t}\frac{M_x}{2A_m} \tag{3.4}$$

which gives the following values

	Section 1	**Section 2**	**Section 3**
τ **[MPa]**	37,7	15,3	7,9

Table 3.6: Shear stress

The shear capacity is according to von Mises yield criterion

$$f_s = \frac{f_y}{\sqrt{3}} = 178MPa \tag{3.5}$$

and we note that

$$\tau_{max} < f_s \tag{3.6}$$

3.6 Buckling Check

As buckling can prove to be the governing failure mode, the tower has to be designed against buckling. The cut-outs of the shell will not be accounted for in the buckling check, but will be further discussed and analyzed in the forthcoming chapter. DNV-RP-C202 is used for the buckling check. This guideline serves as an semi-empirical method, as there in some cases can be significant deviations between theoretical and experimental results. Imperfections and residual stresses from fabrication is taken into account, filling the gap between theoretical and experimental results.

By applying the buckling-guidelines in a spreadsheet, the dimensions can easily be changed to get a usage factor that is adequate. Each section has a length of 23.3 meters and a radius equal to the mean radius of the shell

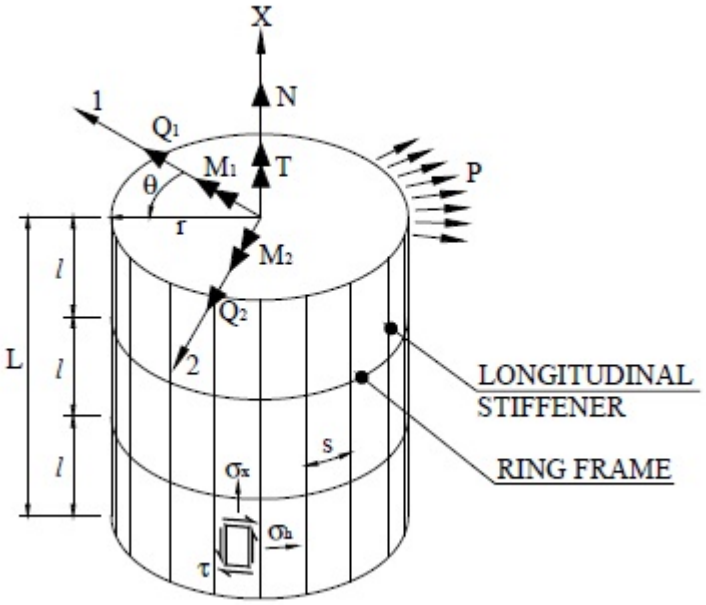

Figure 3.1: Stiffened cylindrical shell

section. This gives the parameters presented in table 3.7 for the buckling check

	Section 1	**Section 2**	**Section 3**
L [mm]	23333	23333	23333
r [mm]	2425	2000	1675
σ_x **[MPa]**	123,5	99,8	69,2
τ **[Mpa]**	37,7	15,3	7,9

Table 3.7: Shell parameters

Experience and earlier analyzes of a similar flare tower[12] shows that the large moment near the bottom of the structure gives large stress concentrations around the cut-outs. This will result in a greater shell thickness than required at this particular section. For the ring stiffeners it is a general requirement for the stiffener area which is

$$A_{req} \geq \left(\frac{2}{Z_l^2} + 0.06\right) lt \tag{3.7}$$

For the longitudinal stiffeners there is a requirement that applies for the

stiffener spacing and thickness ratio

$$\frac{s}{t} > 3\sqrt{\frac{r}{t}} \tag{3.8}$$

The elastic buckling strength for shells is given by

$$f_E = C\frac{\pi^2 E}{12(1-\nu^2)}\left(\frac{t}{l}\right)^2 \tag{3.9}$$

where

$$C = \psi\sqrt{1+\left(\frac{\rho\xi}{\psi}\right)^2} \tag{3.10}$$

By the shell geometry it follows for the upper and mid section that buckling coefficients becomes

Mid section			
Stress	ψ	ξ	ρ
Axial	1,0	274,0	0,3
Bending	1,0	274,0	0,3
Torsion and shear	5,3	75,2	0,6

Table 3.8: Buckling coeff. for mid section

For the top section the following values are calculated

Upper section			
Stress	ψ	ξ	ρ
Axial	1,0	27207,8	0,3
Bending	1,0	27207,8	0,3
Torsion and shear	5,3	2364,5	0,6

Table 3.9: Buckling coeff. for top section

For the bottom section the elastic buckling strength is given by

$$f_E = C\frac{\pi^2 E}{12(1-\nu^2)}\left(\frac{t}{s}\right)^2 \tag{3.11}$$

and the buckling coefficients are

Top section			
Stress	ψ	ξ	ρ
Axial	4,0	5,4	0,4
Torsion and shear	5,6	1,9	0,6

Table 3.10: Buckling coeff. for bottom section

	Section 1	**Section 2**	**Section 3**
t [mm]	23	11	8
s [mm]	700	N/A	N/A
l [mm]	3000	3000	23333
UF	0,57	0,88	0,91

Table 3.11: Shell design

This gives the composition of shell dimensions and stiffeners as presented in table 3.11.

The usage factor on the bottom section is far below the limit and the shell thickness could be even lower to prevent shell buckling. However, a previous study of the cylindrical flare tower [12] shows that stress concentrations occurs at the cut-outs on the bottom section and a larger thickness is set to prevent this phenomenon.

The study shows that there will be no additional stiffening at the top section of the flare tower, but ring stiffeners will be introduced at the mid and bottom section. The bottom section will also get increased capacity due to longitudinal stiffeners.

3.6.1 Ring stiffeners

The ring stiffeners have the sectional attributes as in table 3.12. These dimensions applies both for the bottom and mid section. There are a number of 8 ring stiffeners on each section.

Ring stiffeners			
H	200	$\mathbf{t}_w$	9
B	90	$\mathbf{t}_f$	12

Table 3.12: Ring stiffener dimensions

To avoid water entrapment, L-bar stiffeners were chosen for the ring stiffeners as illustrated in figure 3.2.

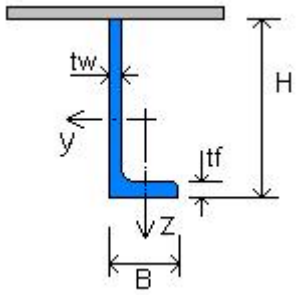

Figure 3.2: Ring stiffeners

If $e_f \neq 0$, the following requirement for flanged profiles is given to avoid local buckling of ring frames

$$\frac{h}{1.35t_w\sqrt{\frac{E}{f_y}}} = 0.87 \leq 1 \tag{3.12}$$

which is well within the safe region in this case.

3.6.2 Longitudinal stiffeners

The longitudinal stiffeners are applied on the bottom section of the tower and counts 22 longitudinal stiffeners.

Longitudinal stiffeners			
H	300	$\mathbf{t}_w$	10
B	200	$\mathbf{t}_f$	15

Table 3.13: Longitudinal stiffener dimensions

Since there is no risk of water entrapment for the longitudinal stiffeners, the characteristic I-profile is chosen.

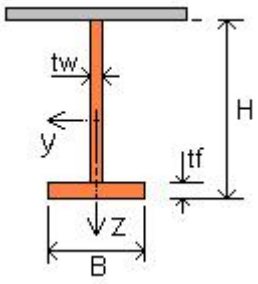

Figure 3.3: Longitudinal stiffeners

The same requirement, as for the ring stiffener, is valid for local buckling of the longitudinal stiffener.

$$\frac{h}{1.35t_w\sqrt{\frac{E}{f_y}}} = 0.64 \leq 1 \tag{3.13}$$

3.7 Weight

The weight of the flare tower is of great importance and will be an important factor when comparing the new design to conventional flare towers. From the previous section, we get that the stiffeners contribute with the following weight.

Weight of stiffeners		
	Ring [T]	**Longitudinal [T]**
Section 1	5,4	11,1
Section 2	4,5	0
Section 3	0	0

Table 3.14: Weight of stiffeners

The cylindrical structure gives a total weight of

Shell weight [T]	
Section 1	64
Section 2	25
Section 3	15

Table 3.15: Shell weight

To account for weight of welding and material imperfections, one can add a total of 2.5 % of the total weight to the structure, which is a conservative approximation. This gives a total weight of 128.6 tonnes.

3.8 Eigenfrequency

The eigenfrequency is for this structure of great interest with respect to VIV and dynamic response. An approximate value can be obtained by using a formula for a cantilever beam[15]. The eigenfrequency is given by

$$\omega_n = \overline{\omega}_n \sqrt{\frac{EI}{ml^4}} \tag{3.14}$$

where the values for $\overline{\omega}_n$ is given by the following values

	n=1	**n=2**	**n=3**
$\overline{\omega}_n$	3,516	22,03	61,7

Table 3.16: Eigenvalue

This gives the first three eigenvalues

	n=1	**n=2**	**n=3**
ω_n **[rad/s]**	8,6	53,7	150,5
f [Hz]	1,4	8,6	24,0

Table 3.17: Approximate eigenfrequency

which seems like a good approximation for the structure.

Chapter 4

ANSYS

4.1 FE-model

For finite element analysis a model was created in ANSYS. The dimensions were determined from a spreadsheet, as shown in the previous chapter. This is to avoid creating a large number of models, as the modelling process is relatively time consuming.

The shell element chosen for the model is named SHELL93 and is from the ANSYS element library. This is an 8-node structural shell element which is more suitable for modelling curved shells than 4-node flat elements. Furthermore, the element is able to represent non-linearities, plasticity and stress stiffening.

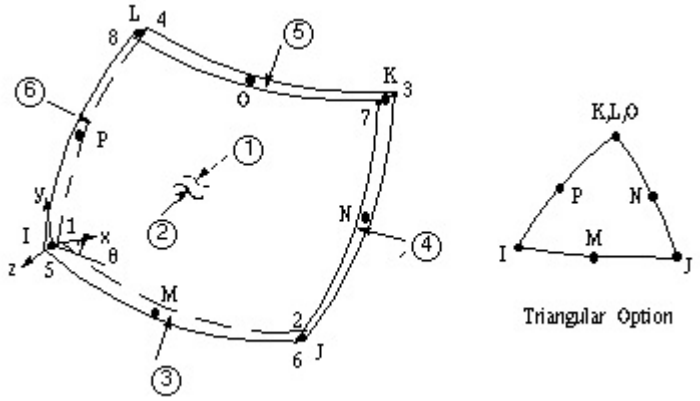

Figure 4.1: Element geometry

The flare tower is inclined 15 degrees in the model and the accelerations can be applied directly without decomposition. The longitudinal and ring stiffeners are not represented in the model, but the equivalent thickness due to longitudinal stiffening is given as the shell thickness for each section. By the formula[3, p. 9]

$$t_e = t + \frac{A}{s} \tag{4.1}$$

the following equivalent thicknesses are obtained

	Bottom section	**Mid section**	**Top section**
t_e **[mm]**	38	11	8

Table 4.1: Equivalent thickness

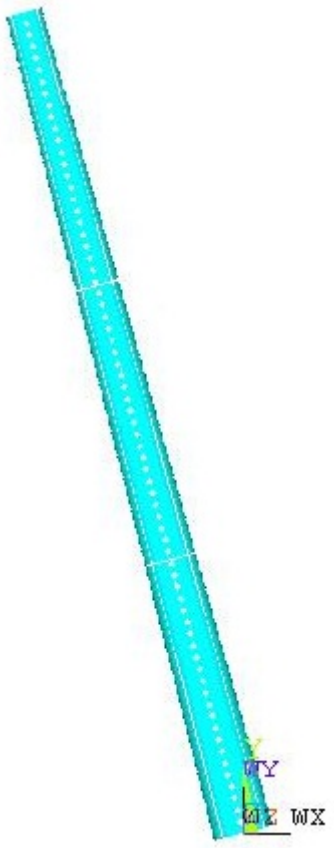

Figure 4.2: Finite Element Model

The finite element model is illustrated in figure 4.2.

4.1.1 Cut-Outs

Due to the large wind pressure acting on the structure, it is beneficial with cut-outs, acting as ventilation for the flare tower. The alignment and positions of the cut-outs can also be used to prevent or limit vortex induced vibrations, which will be a topic of discussion later in the thesis. These cut-outs have a diameter of 0,3 meters, with an elevation of 1 meter between each cut-out. Each section counts four cut-outs with an angle of 90 degrees between each cut-out. However, these cut-outs are often subject to stress concentrations as shown in a previous study[12]. This will be discussed further throughout the thesis.

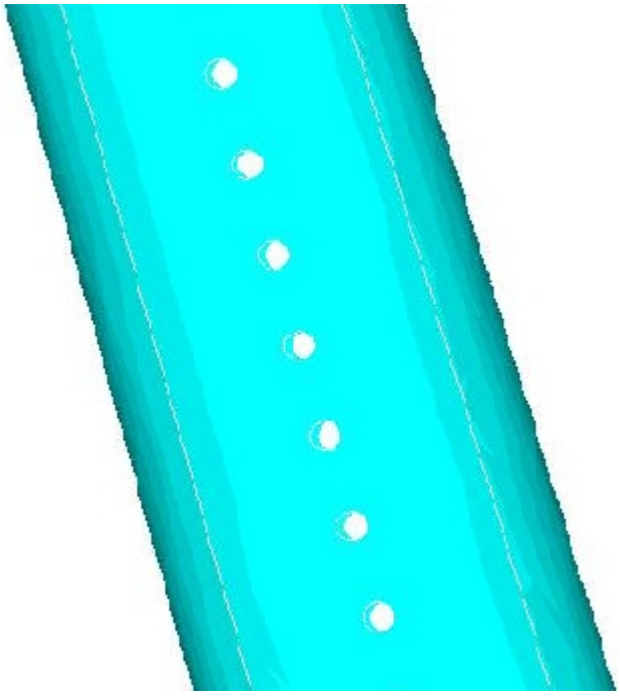

Figure 4.3: Cut-outs

4.1.2 Boundary Conditions

The flare tower is assumed welded to the deck and gives no rotations nor displacements at that particular point. There are no other connections on the structure. As a result of this the boundary conditions are set to fixed to the bottom of the flare tower.

4.1.3 Mesh

A fairly coarse mesh is chosen for the quasi-static and dynamic analyzes. The element length is set to 0,3 meters and quadratic elements are used. As illustrated in figure 4.4, a finer mesh would have been more suitable around the cut-outs, but this will be the subject in another section.

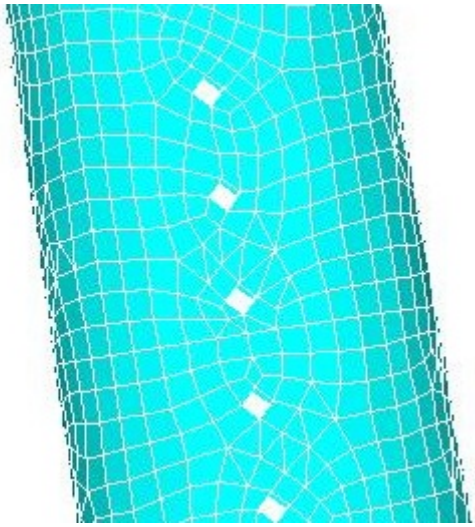

Figure 4.4: Mesh

4.2 Quasi-static Analysis

4.2.1 ULS

The Frøya wind model serves as a quasi-static wind load, with representation of both mean wind pressure and pressure due to wind gusts and wind turbulence. Under a ULS consideration[2], the load cases that are to be examined are the following

Load Combination	**G**	**Q**	**E**	**D**
A	1.3	1.3	0.7	1.0
B	1.0	1.0	1.3	1.0

Table 4.2: Load Factors

- G = permanent load
- Q = variable functional load
- E = enviromental load
- D = deformation load

Load combination B will give far superior loads to those of load combination A, since the enviromental loads will be governing in this case.

The wind pressure are applied on 1/4 of the surface area in the direction of the flare tower inclination, which will be worst case scenario combined with horizontal platform movements in the same direction. Since the wind speed increases rapidly by height, three different pressures are applied by the length of the tower since the wind profile is not linear, and a pressure gradient would be misrepresentative. The mean wind pressure value is used for each section

	Bottom section	**Mid section**	**Top section**
Pressure [Pa]	1455.9	1650.7	1776.1

Table 4.3: Wind pressure ULS

The accelerations to be applied are the following

	Horizontal	**Vertical**
Acceleration $[\mathbf{m}/s^2]$	**3.52**	**3.51**

Table 4.4: Accelerations ULS

The static analysis in ANSYS reveals that the largest stresses occur at the bottom cut-out on the mid section tensile side of the flare tower. This is to some extent expected, since stresses tend to concentrate near the cut-outs. As illustrated the maximum stress is 95,5 MPa.

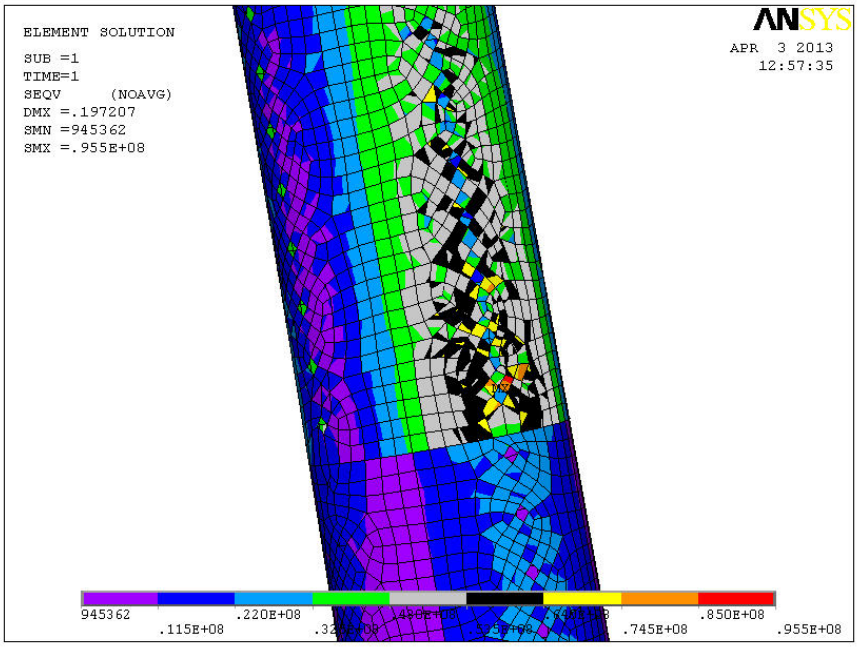

Figure 4.5: Quasi-static Analysis, Von Mises Stress ULS

The largest displacements are found at the top of the flare tower with maximum value of nearly 20 cm. Compared to the overall dimensions of the structure, the displacements are not of an unrealistic magnitude.

4.2.2 ALS

The accidential limit state is also to be investigated. This is a limit state covering the loads corresponding to an annual exceedance probability of 10^{-4}. The material factor and load factors, γ_m and γ_f, are set to 1.0. The 1-hour 10000-year mean wind is chosen for the wind loads giving the following wind pressures

	Bottom section	Mid section	Top section
Pressure [Pa]	1538,3	1754,3	1893,4

Table 4.5: Wind pressure ALS

The accelerations chosen are the 1000-year values, as no other information are available

	Horizontal	Vertical
Acceleration [m/s^2]	**2.51**	**2.30**

Table 4.6: Accelerations ALS

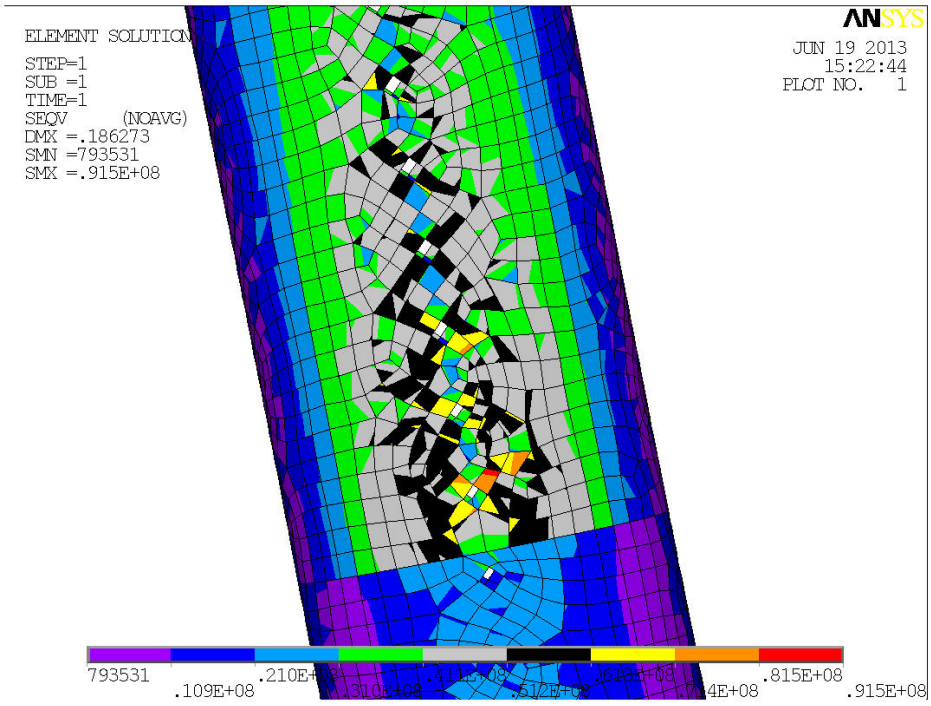

Figure 4.6: Quasi-static Analysis, Von Mises Stress ALS

The maximum Von Mises stress is found to be 91.5 MPa and the largest displacements are 18.6 cm.

4.3 Dynamic Analysis

The response of the structure is an important aspect in structural analysis. The fluctuating wind speed may prove to excite the flare tower in such a manner that the dynamic response will give higher stresses than of those obtained in the quasi-static analysis.

4.3.1 Wind Spectrum

To include the dynamic contribution one does often use a wind specter. There are a large number of existing wind spectra, all in which model the wind gusts. The wind specter chosen in this analysis is the Frøya wind specter. It is a spectrum which is commonly used to describe the North Sea enviroment, since it is a spectrum that models wind over sea, opposed to those who are based on wind over land. This specter describes the energy density of the wind speed fluctuations and is given by

$$S(f) = \frac{320 \cdot \left(\frac{U_0}{10}\right)^2 \cdot \left(\frac{z}{10}\right)^{0.45}}{(1 + \widetilde{f}^n)^{\frac{5}{3n}}} \tag{4.2}$$

where n = 0.468 and

$$\widetilde{f} = 172 \cdot f \cdot \left(\frac{z}{10}\right)^{\frac{2}{3}} \cdot \left(\frac{U_0}{10}\right)^{-0.75} \tag{4.3}$$

The wind pressure specter can be found by using equation 4.4[14]

$$S_w(f) = \frac{4\overline{q}^2 S_v(f)}{\overline{u}^2} \tag{4.4}$$

and is plotted in figure 4.8.

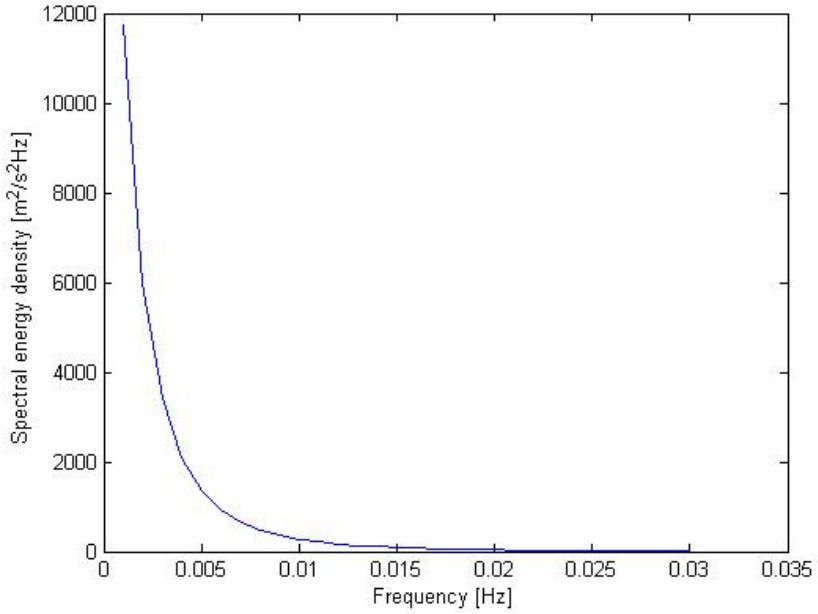

Figure 4.7: Frøya Wind Specter

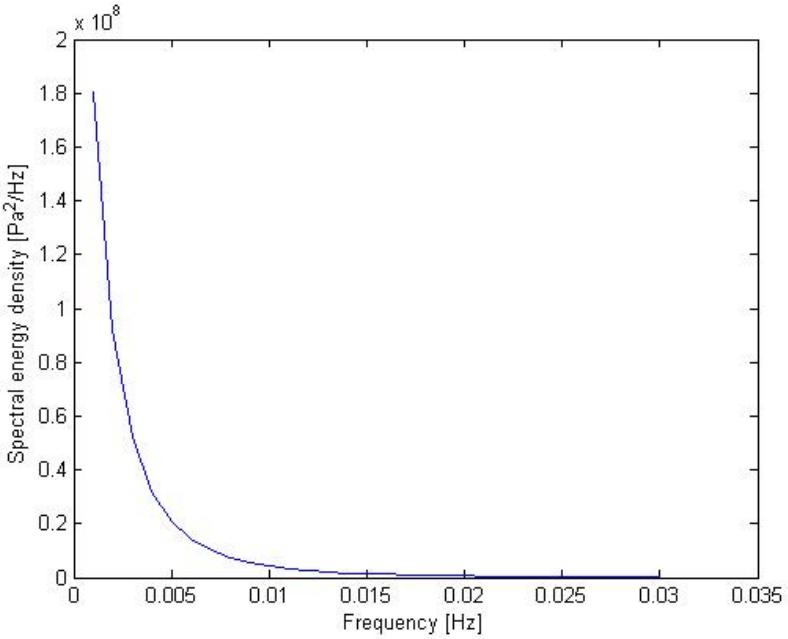

Figure 4.8: Wind Pressure Specter

4.3.2 Eigenfrequency

The eigenfrequencies are calculated in ANSYS utilizing modal analysis. For large symmetric eigenvalue problems the subspace iteration is proposed and chosen for the analysis. In the forthcoming chapters the eigenfrequencies are used for several calculations, which is of great relevance in this assignment. The first 6 eigenfrequencies are presented in table 4.1.

Mode	1	2	3	4	5	6
Eigenfrequency [Hz]	1.7633	1.7663	2.1625	2.1724	3.3147	3.3807

Table 4.7: Eigenfrequencies

4.3.3 Structural Damping

For structures with large degrees of freedom it is difficult to give a good estimate of the α and β values, used for calculating the damping ratio when using Rayleigh-damping. The physical damping of the system is given by [15]

$$C = \alpha M + \beta K \tag{4.5}$$

where M and K is the mass and stiffness matrices, respectively.
In many cases one uses a constant damping ratio for all modes. This will in many cases be unrealistic, since the modal mass participation decreases with increasing modes until nearly 100% mass participation is achieved. A proposed method[13] is used to ensure a good estimate of the Rayleigh coefficients and thus the damping ratio for each mode.

Orthogonal transformations of the damping matrix gives

$$2\lambda_i\omega_i = \alpha + \beta\omega_i^2 \tag{4.6}$$

and hence the damping ratio is given by

$$\lambda_i = \frac{1}{2}\left(\frac{\alpha}{\omega_i} + \beta\omega_i\right) \tag{4.7}$$

A linear relationship for the damping ratio can be obtained by

$$\lambda_i = \frac{\lambda_m - \lambda_1}{\omega_m - \omega_1}(\omega_i - \omega_1) + \lambda_1 \tag{4.8}$$

Under the assumption of a damping ratio of 5% for the first mode and 10%

for the m^{th} significant mode, where in this case m = 10, one uses eq. 4.4 to estimate the damping ratios for the corresponding modes.

For the modes greater than m and to the limit of 2.5m, the damping ratios is obtained by extrapolation

$$\lambda_i = \frac{\lambda_m - \lambda_1}{\omega_m - \omega_1}(\omega_{m+i} - \omega_m) + \lambda_1 \tag{4.9}$$

The β-value can be estimated from

$$\beta = \frac{2\lambda_1\omega_1 - 2\lambda_m\omega_m}{\omega_1^2 - \omega_m^2} \tag{4.10}$$

By back-substituting the β in the expression

$$2\lambda_1\omega_1 = \alpha + \beta\omega_1^2 \tag{4.11}$$

one can obtain the value of α.
This procedure is performed for the following four data sets

- Linear interpolation of the full range of frequencies, using eq. 4.4.
- A set based on the values λ_1, λ_m, ω_1 and ω_m.
- A set based on the values λ_1, $\lambda_{2.5m}$, ω_1 and $\omega_{2.5m}$.
- A last set based on the averages of the two previous data sets.

The routine is performed in MATLAB, as shown in Appendix A, with the start values of $\lambda_1 = 0.05$ and $\lambda_m = 0.10$. This produces the data plot in figure 4.9.

The data set that fits best with the linear interpolation curve for the first m modes will give the α and β values for the structure. From the plot it is obeserved that the first data set, based on the first 10 modes, gives the best fit. Hence, the damping coefficients are

α	β
0,4631	0,0054

Table 4.8: Damping coefficients

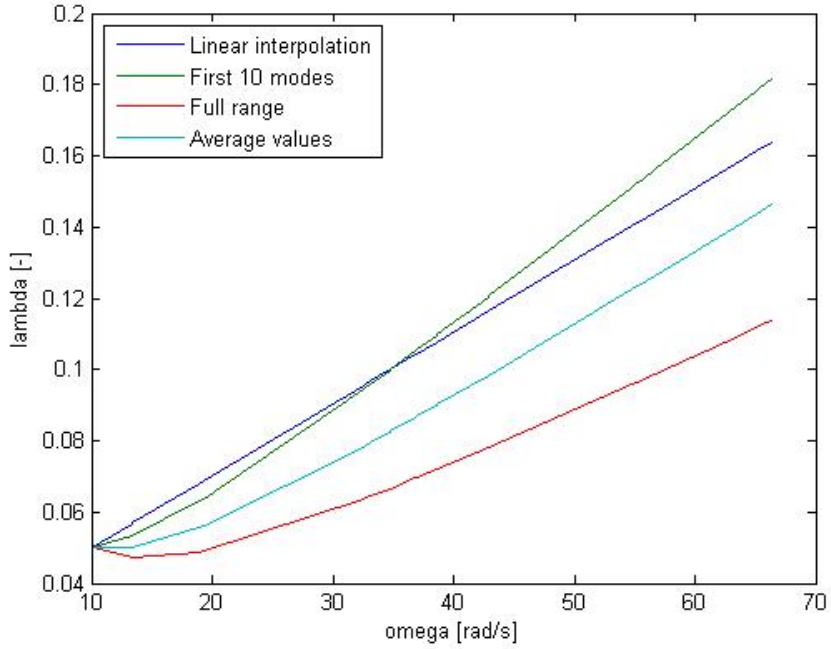

Figure 4.9: Damping Ratio

4.3.4 Random-vibration Analysis

The random-vibration analysis in ANSYS is a probalistic method which means that the output values are not the actual maximum values, but the probability that they take on certain values. Here the wind fluctuations is applied by utilizing the wind pressure spectrum as in figure 4.8. As first step the modeshapes and eigenfrequencies are determined in a modal analysis, but in this case with a unit pressure on the same surfaces as in the quasi-static analysis, to specify the load vectors used in random-vibration analysis. The spectral values and corresponding frequencies are given as input for the dynamic analysis, combined with the mass and stiffness damping coefficients estimated in section 4.3.3. The actual output of the random-vibration PSD analysis are $1-\sigma$ values, representing the stresses that will occur within 68,31%[18] of the load cycles. However, ANSYS applies the Segalman-Reese method[17] to calculate the root-mean square von Mises stresses.

From the random-vibration analysis it follows that the largest stress to occur is 75.8 MPa. The peak Von Mises stresses occurs at resonance with the mode shape asscociated to a eigenfrequency of approximately 11.6 Hz. This is the eigenfrequency corresponding to the 25th mode shape. Since the first mode shape represents the natural deformation pattern, one can

argue that the mode shapes with the higher number, such as 25, would probably not be realistic. However, it is a conservative estimate and proves that the structure is on the acceptable side of the capacity criterion in terms of dynamic response. As illustrated in figure 4.10, the Von Mises Stresses due to dynamic loading is well within the reasonable range, even though the stresses do not converge towards a specific value for the first 25 modes.

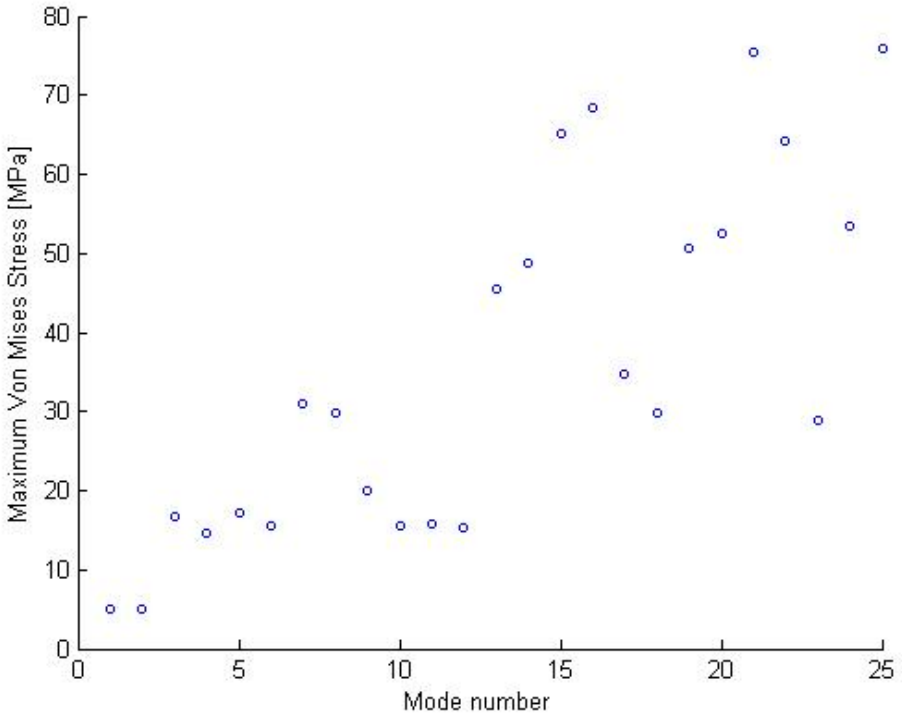

Figure 4.10: Dynamic Stress Plot

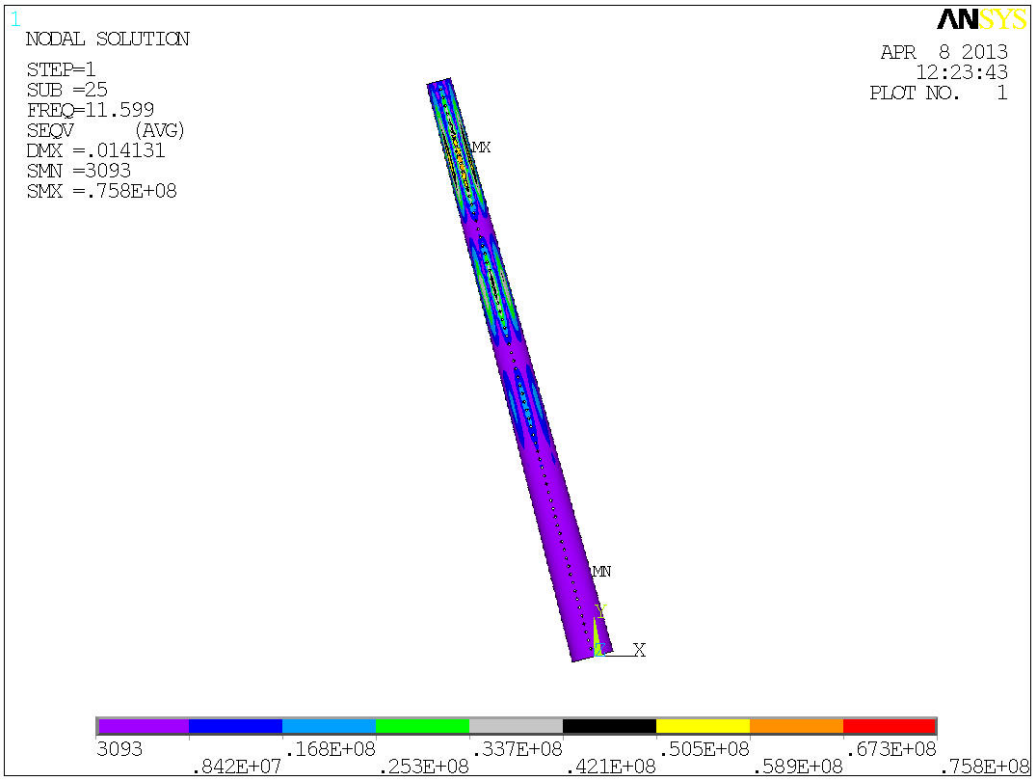

Figure 4.11: Dynamic Von Mises Stress

4.4 Buckling

As a potential collapse mechanism, the buckling strength of the shell needs to be investigated further than the method used in the preliminary design process. To reduce computational time and simplifying the modelling process, the sections between ring stiffeners are chosen for the analyzes. The longitudinal stiffeners are included in the model, opposed to the model used in the quasi-static and dynamic analyzes. The section chosen is not of a conical shape, but with a constant radius to easily compare with the results from the DNV buckling assessment.

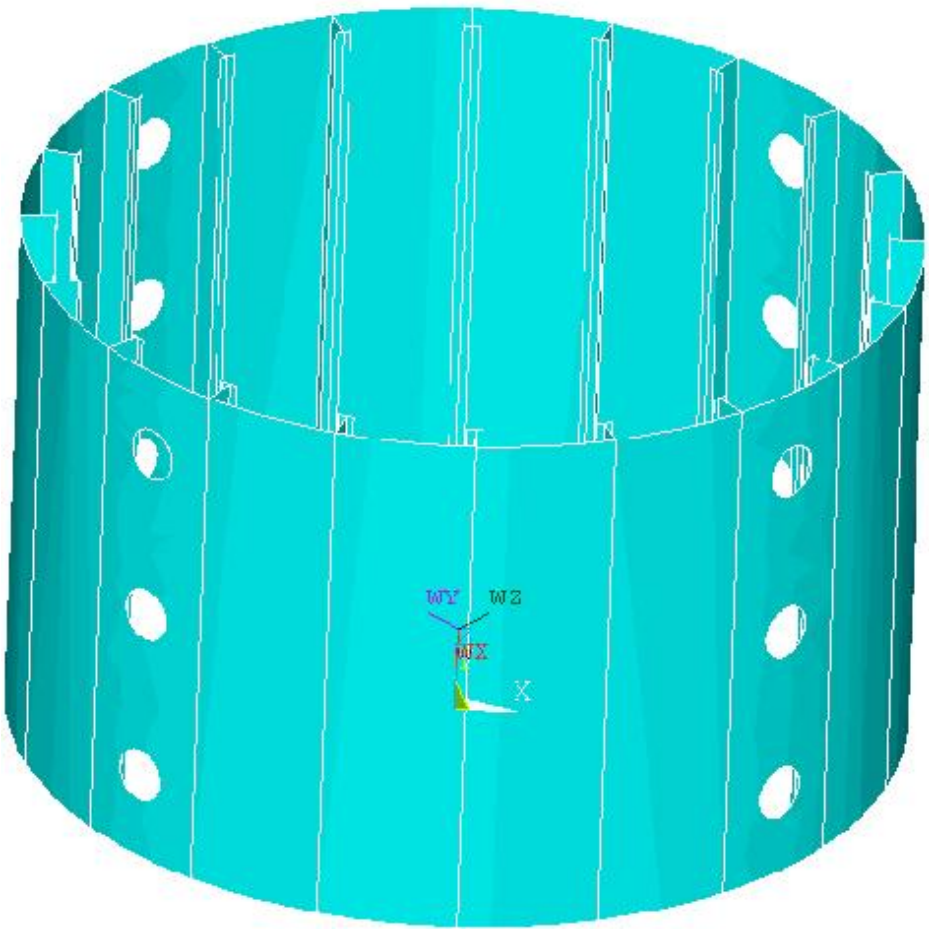

Figure 4.12: Buckling Model

4.4.1 Imperfections

Cylindrical shell elements are highly sensitive to imperfections. Since imperfections always will appear for shell elements, it is beneficial to include these in the finite element analysis. The imperfections are determined by using the highest fabrication tolerance for cylindrical shells i.e. the largest allowed imperfections, according to DNV-OS-C401 Fabrication and Testing of Offshore Structures. From the DNV-rules it follows that the imperfections are given by

$$\delta = \frac{0.01g}{1 + g/r} \tag{4.12}$$

As illustrated in figure 4.13, the length of the circular template, g, should be the smallest of longitudinal stiffener spacing or $\sqrt{l\sqrt{rt}}$.

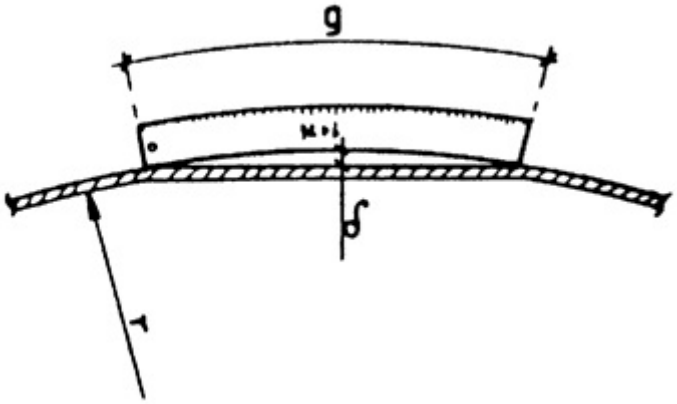

Figure 4.13: Imperfections Geometry

4.4.2 Non-linear Buckling Analysis

The finite elements used in the shell model is of the type shell181. This shell is a 4-node finite strain element well-suited for linear, large rotation, and/or large strain nonlinear application. The shell geometry is illustrated in figure 4.14.

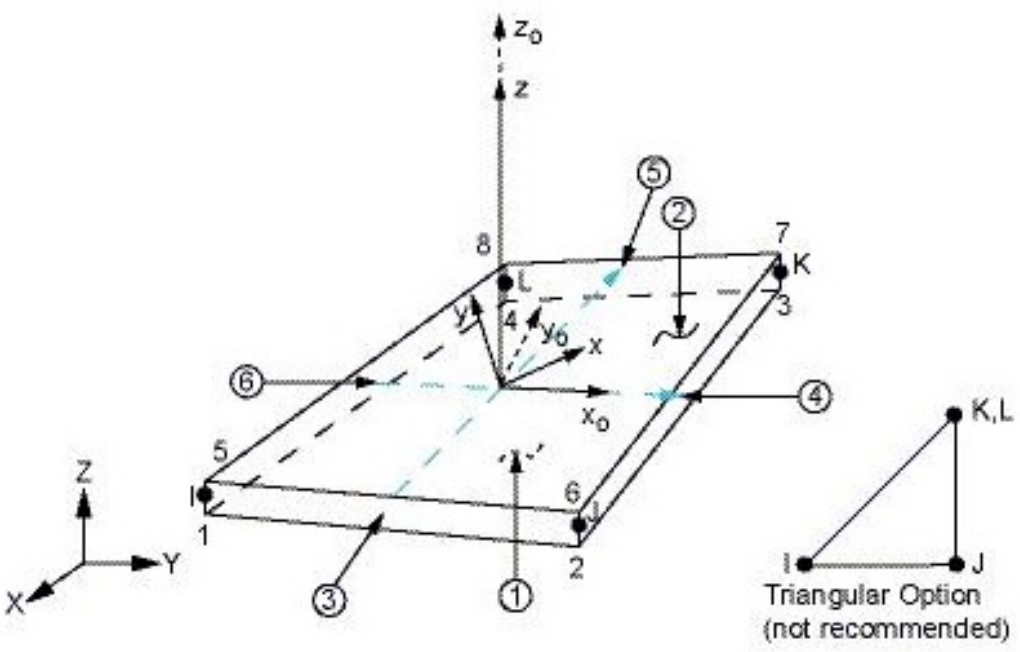

Figure 4.14: Shell181

At the bottom of the cylinder the shell is constrained against both rotations and displacements. On the upper bound of the model, the node displacements follow an element located at the cylinders origin. This element by node connectivity allows the nodes to follow the degrees of freedom specified by the element. A unit pressure gradient is applied at the shell surfaces on the upper boundary. However, this does not give tension on one side and stress on the opposite side of the cylinder as the gradient ranges from 0 to 1. Since the focus only is to predict buckling capacity and the tensile side is not of relevance, the analysis is yet well suited for its purpose. A static analysis with prestress effects is first ran, as the eigenvalue buckling analysis requires the stress stiffness matrix to be calculated. The eigenvalue buckling analysis is ran, giving a small applicable out-of-plane perturbation to perturbation and determening the buckling mode shape. The deformations are later scaled by imperfections found in section 4.4.1. Non-linear

material data is specified and isotropic hardening is chosen as the hardening rule. Isotropic hardening does not account for the Bauschinger effect, stating that an increase in tensile yield strength occurs at the expense of compressive yield strength, as graphically illustrated in figure 4.15. Kinematic hardening does account for this phenomenon. However, reverse loading does not occur during the analysis and isotropic hardening will be satisfactory for representing non-linear material properties. The effect of geometric non-linearities are also included in the analysis.

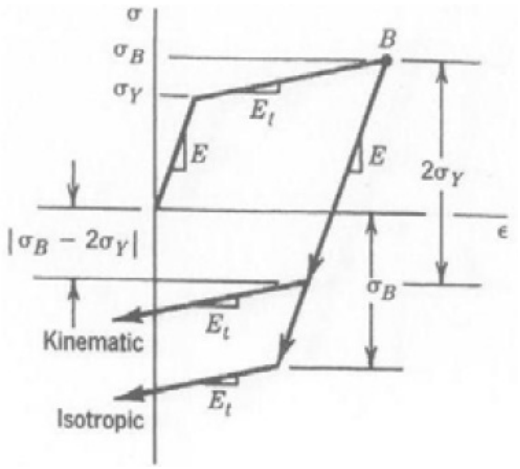

Figure 4.15: Kinematic vs. Isotropic Hardening

The non-linear analysis is conducted to determine the post-buckling behaviour. As the structure reaches its eigenvalue it may prove to have a limit load beyond this point. This phenomenon is called residual strength. By linear buckling one can not reveal the residual strength, as they are triggered by non-linearities. During the non-linear analysis, the applied loads are constantly incremented until the solution begins to diverge. Thus, the last load step gives the predicted buckling strength.

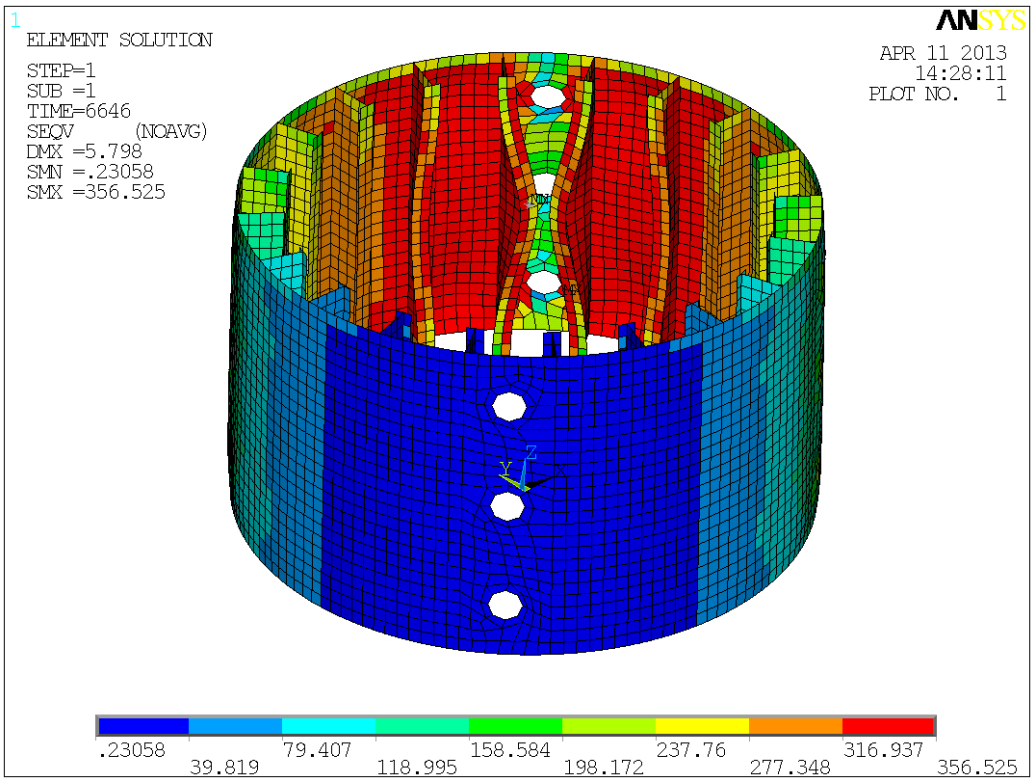

Figure 4.16: Buckling Strength, Bottom

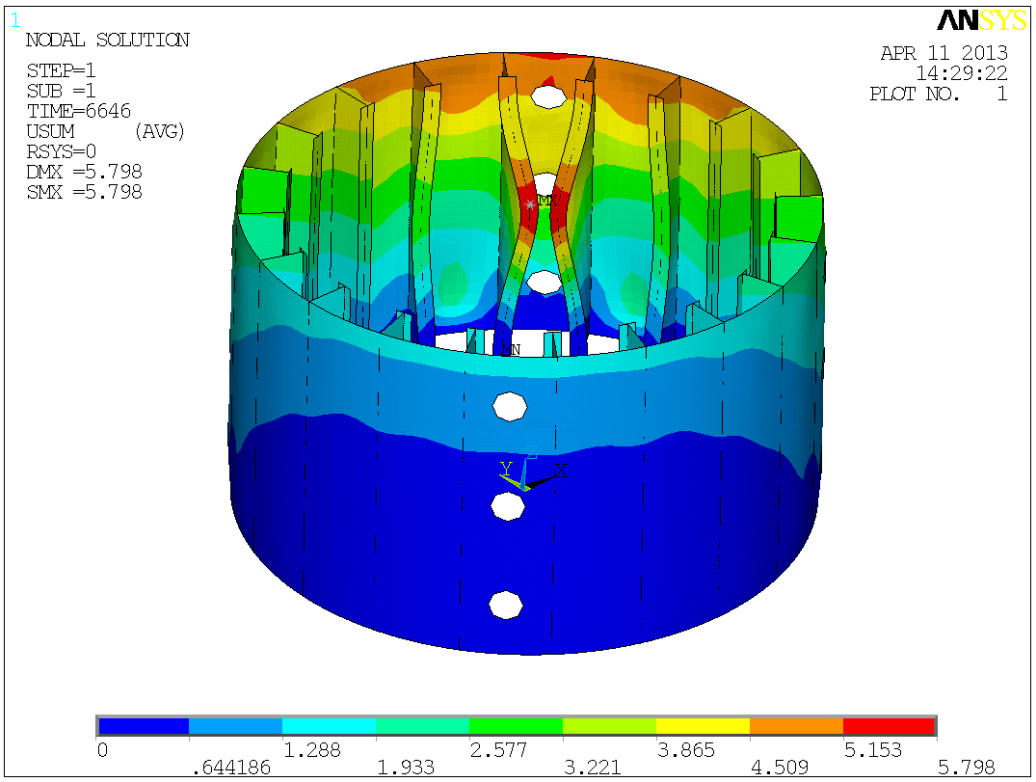

Figure 4.17: Displacements, Bottom

4.5 Mesh Refinement

Convergence with respect to mesh refinement will be of importance when considering a structure with rapid change in geometry. The previous structural analyzes revealed that the stresses tend to concentrate near the cut-outs. The stress gradient around the cut-outs is extremely large compared to the nominal stresses.

A plate in tension is shown in figure 4.18. The tangential stresses for the plate is given by[20]

$$\sigma_\theta = \frac{\sigma}{2}\left[1 + \frac{a^2}{r^2} - \left(1 + 3\frac{a^4}{r^4}\right)\cos 2\theta\right] \tag{4.13}$$

From the equation we see that the maximum stresses occur at r = 0 and $\theta = \pm 90°$ which gives

$$\sigma_\theta = 3\sigma \tag{4.14}$$

The maximum stresses at the edge of the cut-out is therefore 3 times the nominal stresses.

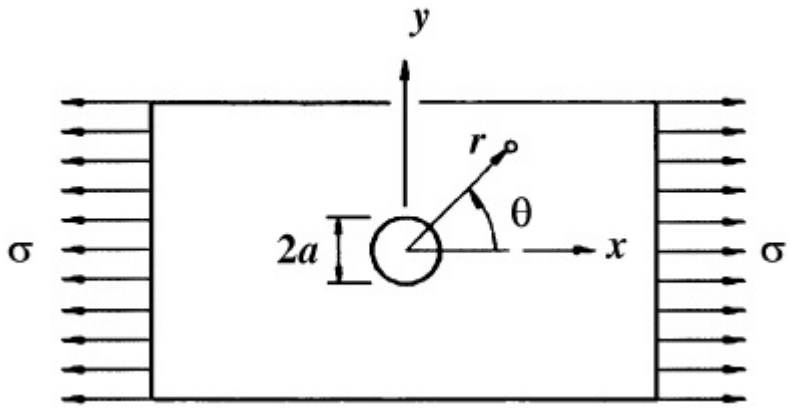

Figure 4.18: Plate Geometry

Given the quasi-static analysis, increasing the mesh refinement from coarse to fine mesh, we can study the convergence of the hot spot stresses. As illustrated in figure 4.19, the stresses will decrease until a fairly fine mesh is established. This might be a result of false geometry, as the coarse mesh fails to model the cut-outs as circles. Applying the mesh with mesh size 50 cm, the cut-out will appear as a triangle. While decreasing the mesh will give a more epliptical shape, until a mesh refinement capable of modeling the cut-outs as circles is established. The epliptical shape will give smaller hot spot stresses, as they will give less rapid change of geometry and thus less stress in accordance to the stress flow analogy. As ANSYS suceeds in modeling circular cut-outs, the stresses converges.

Mesh size [cm]	**Maximum stress [MPa]**	**No. Elements**	**No. Nodes**
50	116	6720	5745
40	113	8394	7550
30	95	13516	13516
20	129	26726	26726
10	145	86768	86768
8	146	120203	120203

Table 4.9: Mesh Refinement

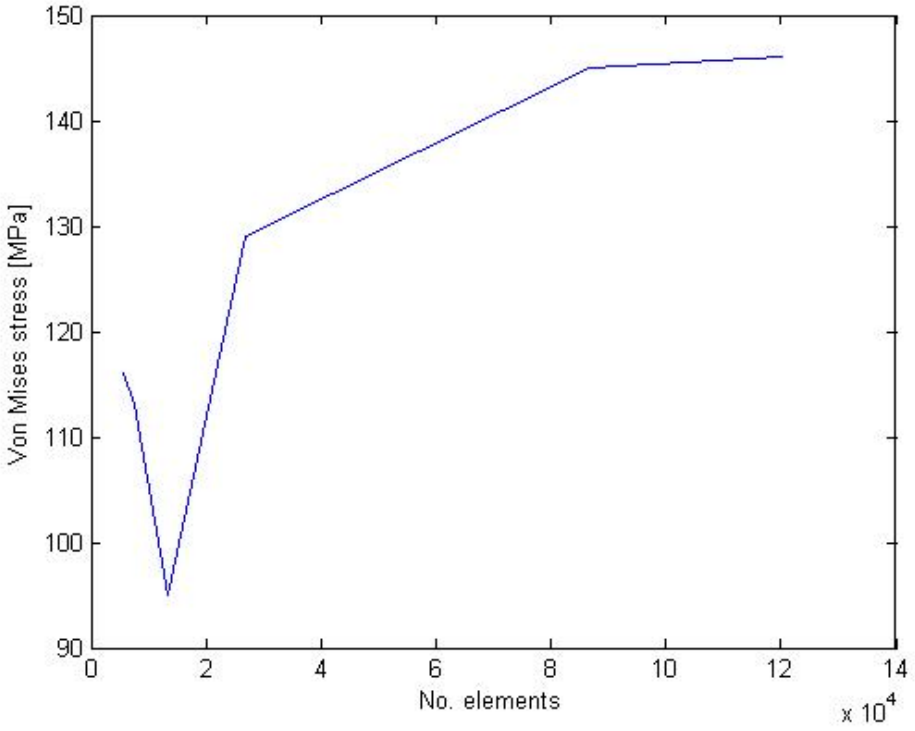

Figure 4.19: Mesh Convergence

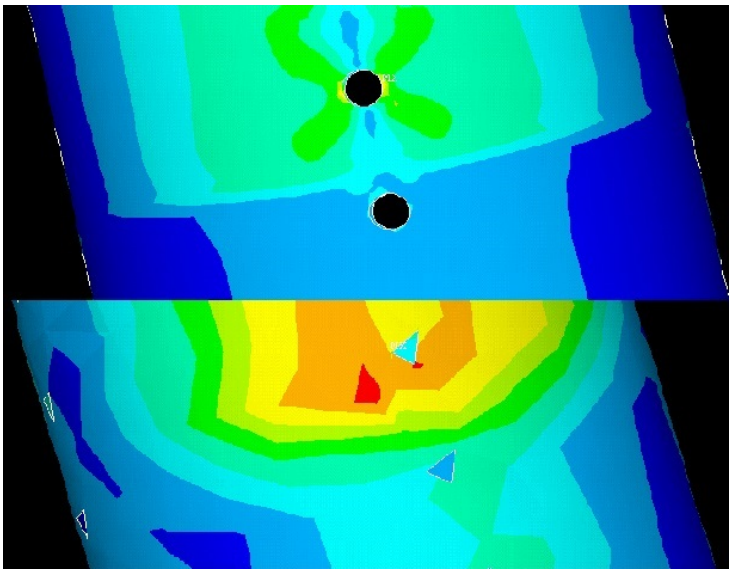

Figure 4.20: Fine vs. Coarse Mesh Geometry

Chapter 5

Vortex Induced Vibrations

For slender offshore structures (e.g. free spanning pipelines, risers, anchor lines), one can often observe vibrations. This phenomenon is called vortex induced vibrations and is associated with the forces developed due to vortex shedding on each side of the cylinder. Large volume structures, such as anchored Spar buoys, may also oscillate due to vortex shedding. This is called vortex induced motions and is characterized as rigid body motions. For the flare tower, elastic motions are most likely to occur and vortex induced vibrations will be of great interest. The forces that occur are defined in in-line and cross-flow direction. That is, perpendicular and normal to the undisturbed incoming flow, respectively. As a result of this, the forces related to CF-vibrations will be of the same frequency as the vortex shedding, while the forces appearing due to IL-vibrations will have their primary frequency at twice the vortex shedding frequency.

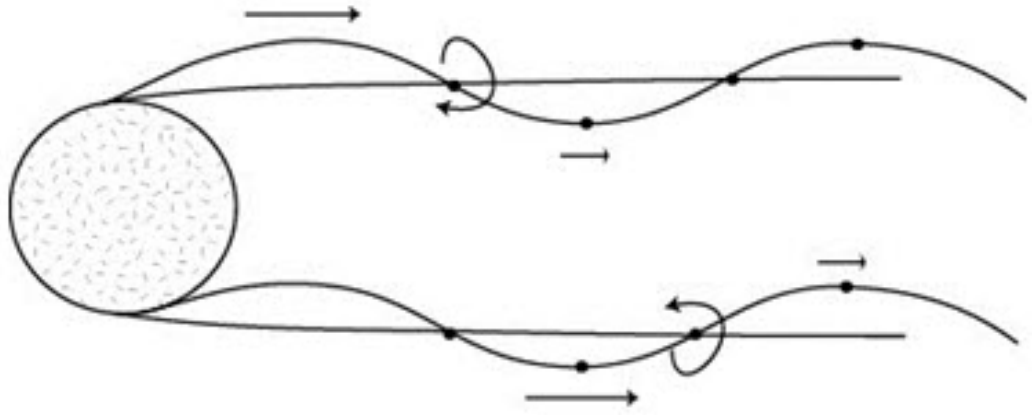

Figure 5.1: Vortex Pattern

The Keulegan-Carpenter number gives the relative importance of drag

forces over inertia forces

$$K_c = \frac{UT}{D} \tag{5.1}$$

For large K_c-numbers drag forces dominate, while for small numbers inertia dominates. According to DNV-RP-C205, the added mass coefficient is given as the maximum value of the two following formulas for $K_c > 3$

$$C_A = 1.0 - 0.044(K_C - 3) \tag{5.2}$$

$$C_A = 0.6 - (C_{DS} - 0.65) \tag{5.3}$$

From figure 5.2 we see that the added mass coefficient reaches its asymp-

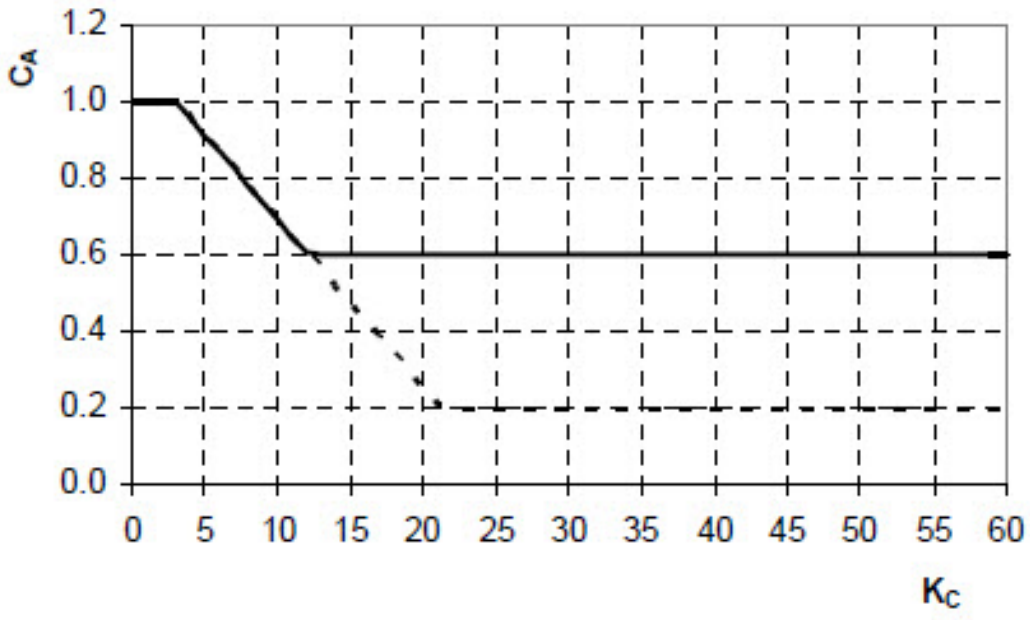

Figure 5.2: Added Mass Coeff. vs. Kc

totic value for large K_c-numbers. The solid lines represent the added mass coefficient for a smooth cylinder. Wind fluctuations will have typically high periods, compared to wave loading, which results in the asymptotic value for the added mass coefficient. The equivalent mass, given as mass per. unit length of the tower, then becomes

$$m_e = m + m_a \tag{5.4}$$

where

$$m_a = C_A \rho_a A_R \tag{5.5}$$

With the equivalent mass calculated, one can determine the stability parameter, K_s.

$$K_s = \frac{2m_e\delta}{\rho_a D^2} \tag{5.6}$$

As proposed by DNV-RP-C205 the logarithmic decrement $\delta = 2\pi\zeta$ can be used, where

$$\zeta = \frac{1}{2}\left(\frac{\alpha}{f_i} + \beta f_i\right) \tag{5.7}$$

using the damping coefficients obtained in section 4.3.3.

When investigating VIV, there are several parameters that are of interest. The vortex shedding is dictated by the Strouhal number which

$$St = \frac{f_s D}{U} \tag{5.8}$$

The Strouhal number is dimensionless number which describes the oscillating flow mechanisms. For a smooth stationary cylinder, the Strouhal number is a function of the Reynolds number. The relationship between Strouhal number and the Reynolds number is shown in figure 5.3.

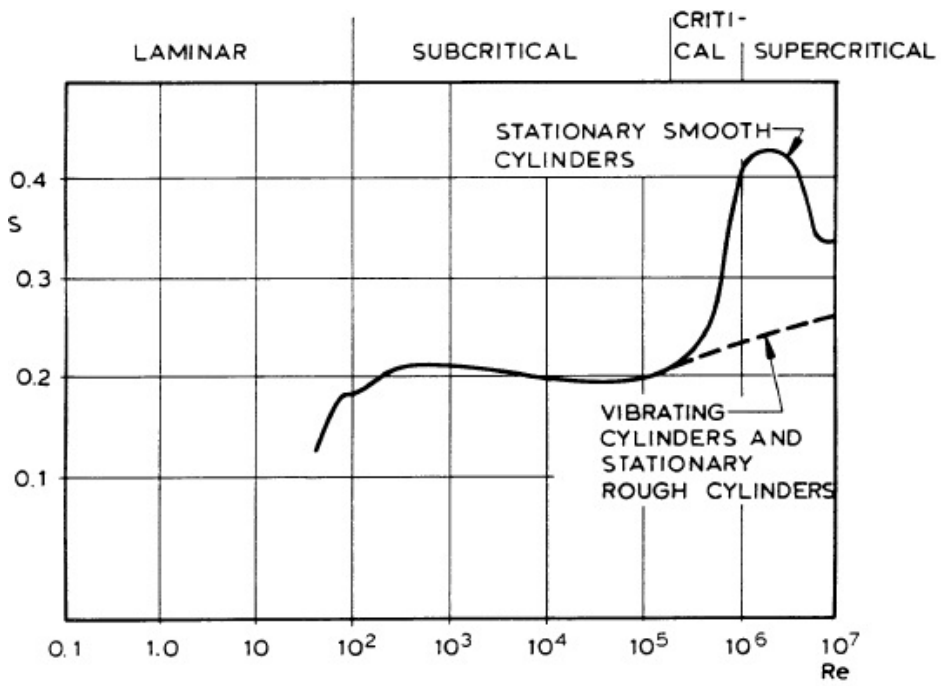

Figure 5.3: Strouhal number as function of Reynolds number

where the Reynolds number is given by

$$Re = \frac{UD}{\upsilon} \tag{5.9}$$

which characterizes the flow regimes (e.g. laminer, turbulent).

5.1 In-line Vibrations

In-line vibrations may occur when[1]

$$\frac{0.3}{St} < V_R < \frac{0.65}{St} \tag{5.10}$$

where the reduced velocity is given by

$$V_R = \frac{U}{f_i D} \tag{5.11}$$

The domain given by equation 5.10 represents the velocity range where the vortex shedding frequency may coincide with the natural frequency given at a given mode shape. This phenomenon is called lock-in, meaning that the vortex shedding process is in resonance with natural frequency, giving vibrations. The lock-in region may be a small fraction of the structure or cover a large extent of the flare tower. Large stability parameters implicates a small lock-in region and/or large damping, which is valid for this case. The parameters used are shown in 5.1.

m [kg/m]	1974,4
m_a [kg/m]	37,0
m_e [kg/m]	2011,4
β	0,0054
α	0,4631
D [m]	4,0

Table 5.1: Values for stability parameter

This retrieves the following stability parameters for the 6 first modes.

Mode	**1st**	**2nd**	**3rd**	**4th**	**5th**	**6th**
$\mathbf{K}_s$	179,96	179,71	154,14	153,66	128,01	127,78

Table 5.2: Stability parameter for 6 first modes

As a simplification, a mean diameter of 4 meters is used for both added mass and directly in calculation of the stability parameter. All calculations are performed in a MATLAB-script as shown in Appendix A. When calculating the Reynolds numbers for the different cross-sections, the routine is looped with an increment of 0.1 meters for the diameter. The corresponding heights and wind speeds, utilizing the Frøya wind model, are found for each increment. This proves that the flow is consistently past the critical regime, with $R_e > 10^7$ for all sections. As a result of this the Strouhals number is set to 0.34. Hence, the reduced velocity range in eq. 5.10 becomes

$$0.88 < V_R < 1.92 \tag{5.12}$$

Now, calculating the reduced velocity for the first 6 modes shows that the stucture is not within the range of lock-in for pure IL-vibrations. Regardless of the forementioned, it is known that in-line vibrations only will occur for $K_S < 2$ [1, pp. 92].

5.2 Cross-flow Vibrations

The critical domain for cross-flow vibrations is given by

$$\frac{0.8}{St} < V_R < \frac{1.6}{St} \tag{5.13}$$

Using the Strouhal number found in section 5.1, one obtains

$$2.35 < V_R < 4.71 \tag{5.14}$$

The MATLAB calculations shown in Appendx A shows that lock-in may occur and give resonant effects for the 5th and 6th mode shape. The lock in region will span from the bottom of the deck up to 53 meters along the flare tower. To determine the cross-flow amplitude one can benefit from the relationship between the stability parameter and the cross-flow amplitude. The relationship is illustrated in figure 5.4 and follows the equation

$$\frac{A_{CF}}{\gamma D} = \frac{0.31}{\sqrt{0.062 + 0.077K_s^2}} \tag{5.15}$$

where the shape parameter is given by

$$\gamma = y_{max}\left[\frac{\int_0^L y^2(x)dx}{\int_0^L y^4(x)dx}\right]^{1/2} \tag{5.16}$$

The mode shape is, by a rather simplified approach, given by[19, pp. 217]

$$y(x) = \frac{\sin \frac{n\pi x}{2L}}{\sin \frac{n\pi}{2}} \tag{5.17}$$

which corresponds to the mode shape for a fixed-free bar element. This gives the following values for the 6 modes.

Mode	**1st**	**2nd**	**3rd**	**4th**	**5th**	**6th**
γ	1.572	1.549	1.575	1.575	1.572	1.572

Table 5.3: Mode shape parameters

The cross-flow amplitudes for the mode shapes in which lock-in will occur are found to be

Mode	**5th**	**6th**
A_{CF} **[mm]**	40.4	40.5

Table 5.4: Cross-flow amplitudes

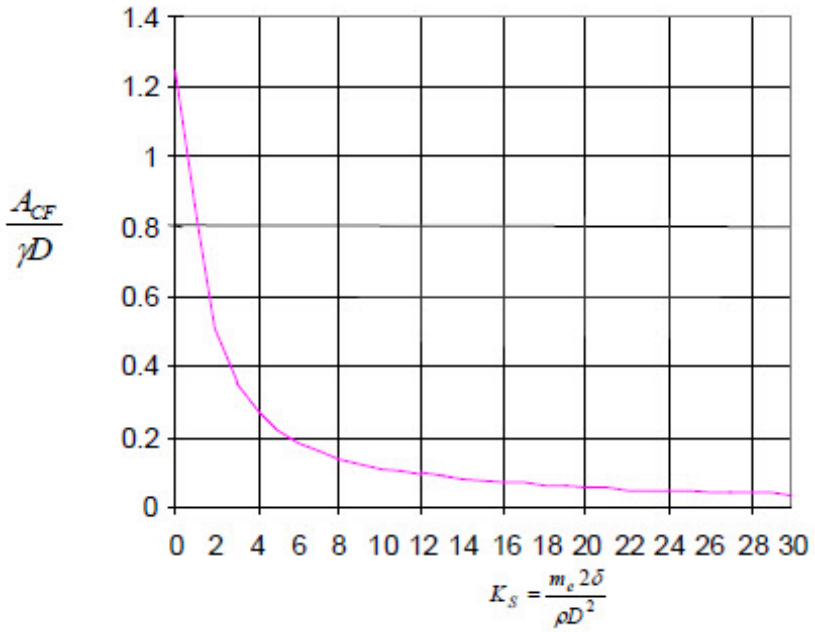

Figure 5.4: Cross-flow amplitude as function of Ks

Chapter 6

Fatigue

The possibility of failure due to cyclic loading needs to be examined. Repeated loading and unloading can result in microscopic cracks at stress concentrations, which again can lead to premature failures. An adequate fatigue life needs to be established, which will also form the basis for inspection programmes.

The dynamic contributions from wind, platform motions and VIV will be the contributers. As covered in section 4.2, the largest stresses will occur near the cut-outs, while the main contribution most likely will be the wind load.

6.1 Dynamic Loading

The quasi-static wind model has proven to give the largest stresses. The stresses obtained from the fluctuating wind pressure, combined with the amplitudes for horizontal and verical platform movements are used in ANSYS. Displacements found in section 5.2 is used to determine the stresses from the VIV-amplitudes. No pure in-line vibrations was found in the VIV-analysis, yet cross-flow induced in-line vibrations may occur at a magnitude of 30-50% of the cross-flow amplitudes. From the previous conducted parametric study, an appropriate mesh size of 8 cm is used, in order to obtain accurate hot spot stress around cut-outs. The dynamic wind pressure is given as

$$q = \frac{1}{2}\rho_a U_{T,z} u \tag{6.1}$$

where the wind speed is the 100-year wind speed provided in table 2.1. The applied pressures and accelerations are presented in table 6.1 and 6.2, respectively.

	Bottom section	**Mid section**	**Top section**
Pressure [Pa]	505.3	500.1	495.9

Table 6.1: Dynamic wind pressure

	Horizontal	**Vertical**
Acceleration [m/s^2]	**2.71**	**2.70**

Table 6.2: Fatigue, Accelerations

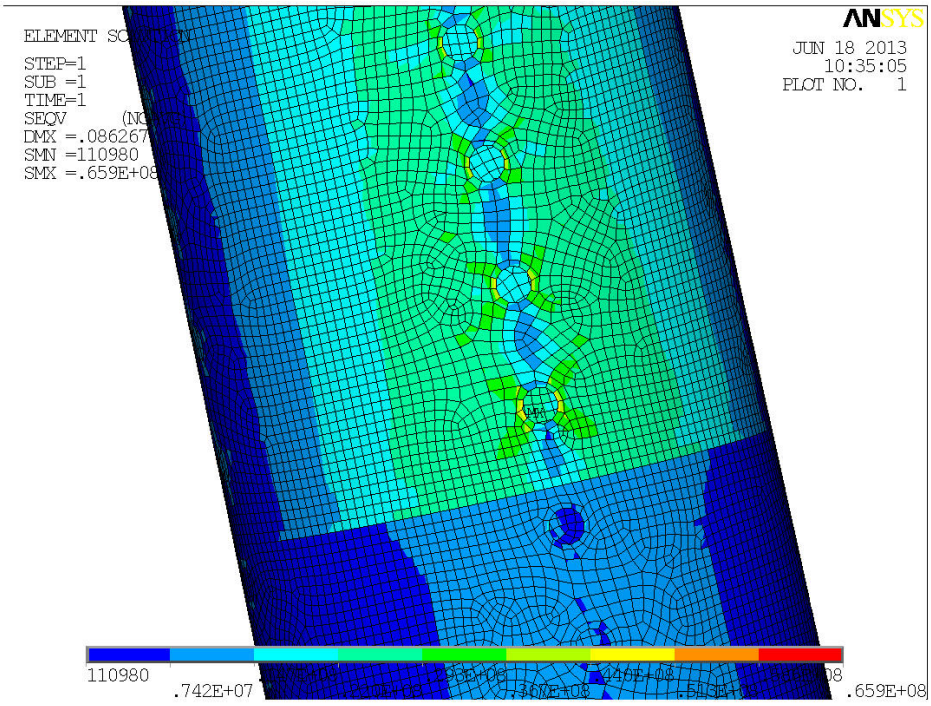

Figure 6.1: Stresses from Dynamic Loads

Various scenarios regarding heading and load direction are explored. The combination giving the largest stresses is wind in the direction of the tower inclination, while the displacements due to VIV will have their natural direction related to the incoming wind. However, the VIV-amplitudes are small, merely giving a contribution to the Von Mises stresses. From the the plot in figure 6.1 the hot spot stress is located in the mid section of the flare tower and is approximately 66 MPa.

6.2 Fatigue Analysis

The fatigue design is based on S-N curves. These curves are derived from fatigue testing of small specimens in test laboratories. From DNV-RP-C203[5], it follows that the practice is valid for, among other failure modes, fatigue crack growth from a surface irregularity or notch into the base material, which is suitable for our case. As the initiation of a fatigue crack takes longer time close to the cut-outs or close to a notch than for welded connenections, the S-N data is divided into several classes. An appropriate class for our structural detail will be class C.

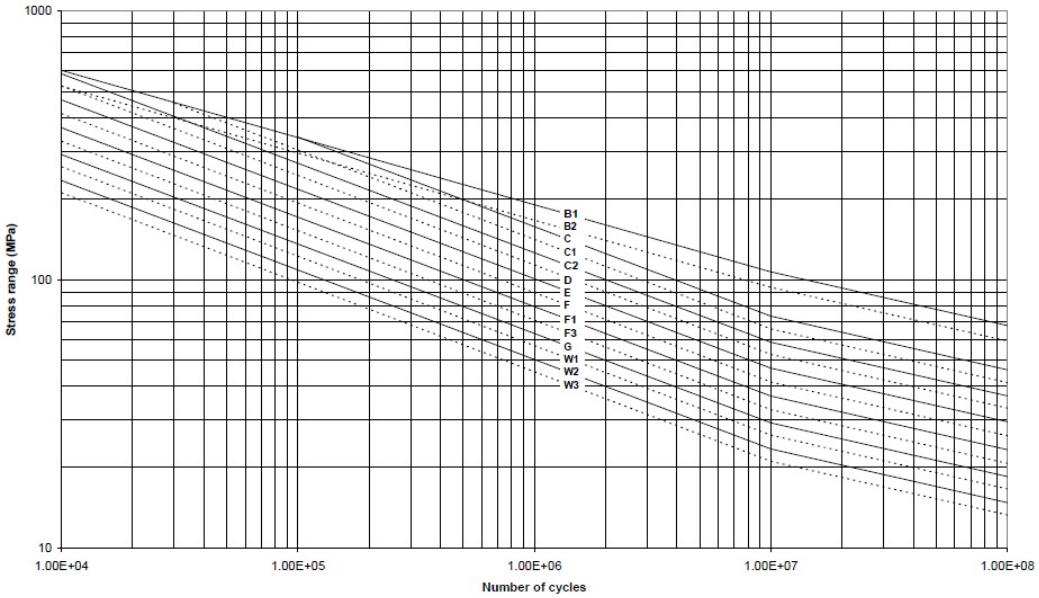

Figure 6.2: S-N Curve Air

The S-N curve follows the following relationship

$$logN = log\overline{a} - mlog\Delta\sigma \tag{6.2}$$

or, alternatively

$$N = \overline{a}\Delta\sigma^{-m} \tag{6.3}$$

where $log\overline{a} = loga - 2s$.

Now, the long term distribution for the stress range needs to be organized in stress blocks. First, lets assume the probability density function of stress range may be represented by a two-parameter Weibull distribution[21]

$$f(\Delta\sigma) = \frac{h}{q} \cdot (\frac{\Delta\sigma}{q}^{h-1}) \cdot exp(-\frac{\Delta\sigma}{q})^h \tag{6.4}$$

Here, we want to eliminate the Weibull parameter q by introducing the maximum stress range $\Delta\sigma_0$. The probability of exceedance of $\Delta\sigma$ is given by

$$Q(\Delta\sigma) = 1 - \int_0^{\Delta\sigma} f(\Delta\sigma) d\Delta\sigma \tag{6.5}$$

By combining equation 6.4 and 6.5 and integrating gives the following exceedance function

$$Q(\Delta\sigma) = exp - (\frac{\Delta\sigma}{q})^h \tag{6.6}$$

The probability that the maximum stress range $\Delta\sigma_0$ is reached or exceeded for n_0 is

$$Q(\Delta\sigma_0) = \frac{1}{n_0} \tag{6.7}$$

combined with eq. 6.6 yields

$$\frac{1}{n_0} = exp - (\frac{\Delta\sigma_0}{q})^h \tag{6.8}$$

and by substituting equation 6.8 into 6.6 we get

$$Q(\Delta\sigma) = \frac{n}{n_0} = exp - \left[(\frac{\Delta\sigma}{\Delta\sigma_0})^h \cdot \ln n_0 \right] \tag{6.9}$$

For the number of cycles n that exceeds $\Delta\sigma$

$$Q(\Delta\sigma) = \frac{n}{n_0} = exp - \left[(\frac{\Delta\sigma}{\Delta\sigma_0})^h \cdot \ln n_0 \right] \tag{6.10}$$

and thus we get

$$\Delta\sigma = \Delta\sigma_0 \Big[1 - \frac{\log n}{\log n_0} \Big]^{1/h} \tag{6.11}$$

The assumed lifetime of the flare tower is 20 years. Since the flare tower is an external structure not accessible for inspection and repair in dry and clean conditions, the design fatigue factor is set to 2. Now, we are set to create a stress histogram. A simplified approach is used, obtaining the stresses that will eventually lead to failure at the treshold of 20 years. When generating the stress histogram the stress range is stepped, and the corresponding cycles can be found by using equation 6.11. This gives

$$n_{i-1} = 10^{\left(\left(1 - (\frac{\Delta\sigma_{i-1}}{\Delta\sigma_{20}})^h \right) \cdot \log n_i \right)} \tag{6.12}$$

$$n_{i+1} = 10^{\left(\left(1-(\frac{\Delta\sigma_{i+1}}{\Delta\sigma_{20}})^h\right)\cdot\log n_i\right)} \tag{6.13}$$

$$n_i = n_{i-1} - n_{i+1} \tag{6.14}$$

The routine is effectively performed in a spreadsheet. From the S-N curve we get the following S-N data

	$N < 10^6$	$N > 10^6$
log (a)	12.592	16.32
m	3	5
k	0.15	0.15

Table 6.3: S-N data

Now, assuming high cycle fatigue with n = 1.0E+08 and a conservative value for the Weibullparameter, h = 1.0, the accumulated damage can be found from

$$D = \sum_{i=1}^{k} \frac{n_i}{N_i} = \frac{1}{a}\sum_{i=1}^{k} n_i(\Delta\sigma)^m \leq \eta \tag{6.15}$$

where the usage factor is divided by the DFF, giving $\eta = 0.5$. From the spreadsheet calculations, the 20 year lifetime, or $D = 0.5$, is achieved with a hot spot stress at 287 MPa. This is higher than the stresses obtained in section 6.1, $\Delta\sigma = 2 \cdot 66MPa$, which implies that the structure is well within the acceptable domain with respect to fatigue.

6.3 Alternative Cut-Out Design

Stress concentrations are often a subject for fatigue, as these hot spot stresses under cyclic loading can lead to initiation of fatigue cracks. Minimization of stress concentrations could prove to be benefitial in order to avoid oversized design. Opposed to the general idea of strengthening areas where stresses tend to concentrate, there are other design methods that could result in a reduction of required material. The geometric stress concentrations that are revealed from the FEM-analysis are due to the rapid change of geometry. Keeping in mind that the governing field equations for ideal irrotational fluid flow are quite similar to those for stress, one could examine a plate element subjected to stress flow. In figure 6.3 from Roark's[20], we see that the streamlines approach the cut-out in a uniform flow at point A. By examining

point B, we observe that the particles close to streamline 1 will have to make a great adjustment, thus accelerating until reaching point c. The compaction of the streamlines leads to a pressure gradient. This will eventually lead to large local stresses at point c.

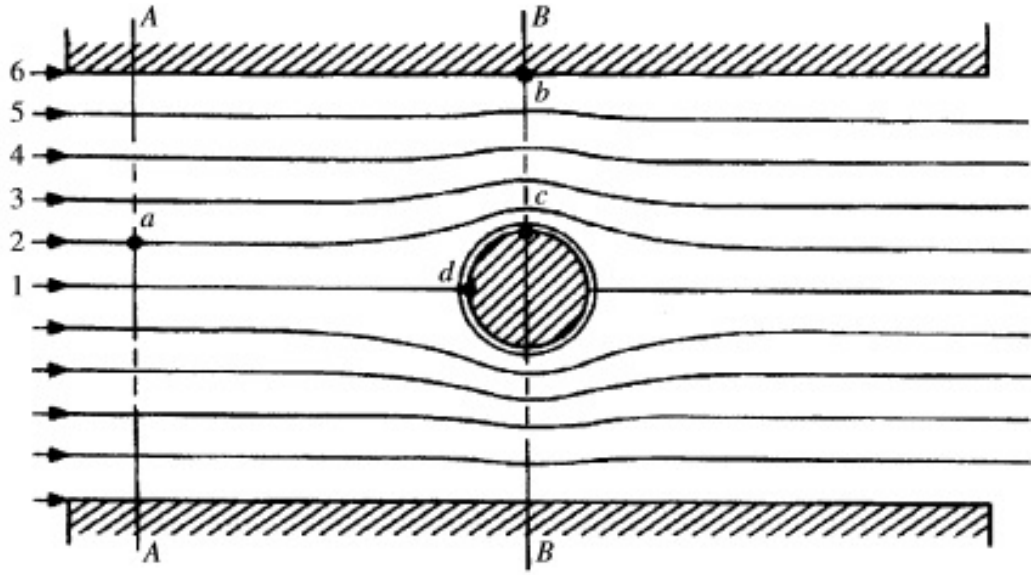

Figure 6.3: Stress Flow

By the previous argument, it follows that a smoother change of geometry will lead to smaller stress concentration along the edge of the cut-out. An epliptical design could be an option, but in many cases not practical. However, the epliptical shape can be approximated by creating small relief holes close to the cut-outs as illustrated in figure 6.4.

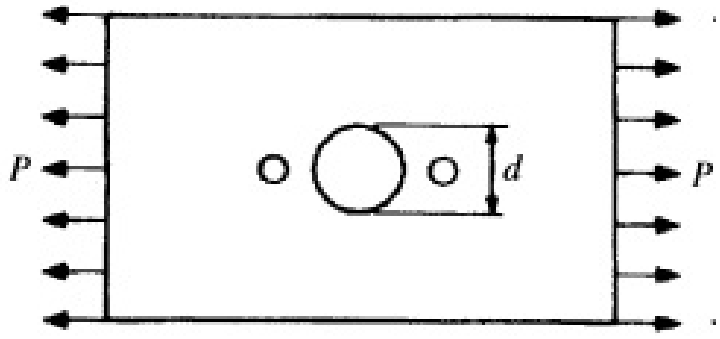

Figure 6.4: Relief Holes

Chapter 7

Discussion

Throughout the thesis various analyzes states that the concept of the novel flare tower design has great potential. The cylincrical flare tower proves to have sufficient strength capacity with respect to all relevant collapse mechanisms. However, as a concept study the design presented in the thesis is not a definite design. If such a concept should be adapted to a practical problem, there may be several other parameters(e.g. environmental data, FPSO/platform design, regulations) that will govern the design.

The preliminary design process is conducted to establish the main dimensions of the tower. This is to avoid generating several finite element models, which is relatively time consuming. The environmental loads are chosen to represent the north sea environment, which is a fairly harsh environment. Some simplification are done in the finite element analysis. As the wind speed increases rapidly by height, the mean values for each section are used. This approximation will give stresses close to those excpected when applying a full wind profile, which proved to be difficult. The random vibration method is used to find the maximum response, utilizing a wind spectrum and damping coefficients calculated. The response is relatively low and the tower proves to be able to withstand a random excitation. However, more realizations of the wind spectrum(e.g. Monte Carlo approach) could have been applied to examine the effect of statistical variation. If the flare tower was to be applied at a specific offshore structure, a more detailed analysis of the structural response should be considered, as the flare tower is generally affected by the response of the rig/platform. The buckling analysis revealed some unexpected findings with respect to residual strength. It is not any general method of predicting residual strength, but the non-linear analysis showed a much larger capacity than the linear analysis. The cause may be that the linear analysis is a general practice, not able to represent all types of shell structures. To determine the lifetime of the structure, a fatigue anal-

ysis was conducted. VIV-amplitudes were calculated and found to be fairly small. This was to some extent expected due to the large diamter of the structure. The fatigue analysis is very conservative as the same heading and wind direction is assumed throughout the whole lifetime of the structure.
The flare tower appear to have oversized design and further optimization should be considered. Although the nominal stresses found from FEA were low, the stress concentrations proved to be large. However, the fatigue analysis proved that the stress concentrations was on the acceptable side and since weight will be an important parameter when designing such a structure, further reduction of material would be necessary. The production of the flare tower will be less labour intensive, with few joints and welds. This proves that the concept is feasible and could compete with traditional flare towers.

Chapter 8

Further Work

Some topics can be further examined as the flare tower concept is far from fully developed. An optimization of the tower is time consuming, with different dimensions and/or arrangements to be considered. Here follows some of the recommendations, apart from designing a cylindrical flare tower for a specific location.

- Transient dynamic analysis with implementation of seed numbers accounting for the effect of statistical variation
- Fatigue analysis based on dynamic load history
- Alternative shape of cut-outs, giving less stress concentrations and further reduction of steel
- CFD-analysis to determine VIV and flow pattern

Bibliography

[1] Det Norske Veritas, Recommended Practice DNV-RP-C205, 2010

[2] Det Norske Veritas, Offshore Standard DNV-OS-C101, 2011

[3] Det Norske Veritas, Buckling Strength of Shells DNV-RP-C202, 2010

[4] Det Norske Veritas, Fabrication and Testing of Offshore Structures DNV-OS-C401, 2010

[5] Det Norske Veritas, Fatigue Design of Offshore Steel Structures, DNV-RP-C203, 2005

[6] NORSOK Standard, N-001 Structural Design, Rev. 4, February 2004

[7] NORSOK Standard, N-003 Actions and Action Effects, 2nd edition 2007

[8] NORSOK Standard, N-004 Design of Steel Structures, Rev. 2 october 2004

[9] NORSOK Standard, M-120 Material Data Sheet for Structural Steel, Edition 5 2008

[10] Statoil, Statfjord Late Life Metocean Design Basis, Kenneth J. Eik and Einar Nygaard, 2003

[11] Sea Loads on Ships and Offshore Structures, Odd Magnus Faltinsen, 1990

[12] Modelling and Analysis of a Cylindrical Flare Tower, Kjetil Legard, 2012

[13] Computation of Rayleigh Damping Coefficients for Large Systems, Indrajit Chowdhury and Shambhu P. Dasgupta, 2003

[14] Simulation of Fluctuating Wind Pressure for Heliostat by Autoregressive Model Method, Ying-ge Wang, 2007

[15] Svingning av kontruksjoner, Pål G. Bergan, Per Kr. Larsen and Egil Mollestad, 1993

[16] Dimensjonering av stålkonstruksjoner, Per Kr. Larsen, 1993

[17] An Efficient Method for Calculating RMS von Mises Stress in a Random Vibration Environment, Daniel J. Segalman, Clay W. G. Fulcher, Garth M. Reese and Richard V. Field Jr., Sandia National Laboratories 1998

[18] Analyzing Random Vibration Fatigue, Santhosh M. Kumar, ANSYS India 2008

[19] Programming the Dynamic Analysis of Structures, P. Bhatt, 2002

[20] Roark's Formulas for Stress and Strain, Warren C. Young and Richard G. Budynas, 7th Edition, 2002

[21] Fatigue Handbook Offshore Steel Structures, A. Almar NÃęss et al., 3. Impression, 1999

Appendix A

MATLAB Scripts

```
%FRYA WIND MODEL
clear all;

%Wind period
T = 15;
%Mean wind speed
U0 = 46;
%Height above sea level
H = 88;
%Mean value used for spectum
z = 59;
%Air density
rho_a = 1.226;

%Wind gusts and profile
C = (5.73E-2)*sqrt(1+(0.148*U0));
for i = 1:H
Iu(i) = 0.06*(1+(0.043*U0))*(i/10)^(-0.22);
Uz(i) = U0*(1+(C*log(i/10)));
u(i) = Uz(i)*(1-(0.41*Iu(i)*log(T/3600)));
end

%Normalized logarithmic design wind profile
lp = u/U0;

%Wind profile plot
for i = 1:H
    x(i) = i;
end

%Wind profile plot
plot(u,x)
```

```
xlabel('u(z,t) [m/s]')
ylabel('Height [m]')

%Fluctuation component
for i = 1:H
    u_flu(i) = u(i) - Uz(i);
end

%Dynamic wind pressure
for i = 1:H
    q_dyn = 0.5*rho_a*u_flu(i)*Uz(i);
end

%Dynamic wind speed plot
%plot(a,u_dyn)
%xlabel('frequency [Hz]')
%ylabel('u(f) [m/s]')

%Static wind pressure
for i = 1:H
    q_stat(i) = 0.5*rho_a*u(i)^2;
end

%Dynamic wind speed plot
plot(x,u_flu)
xlabel('Height [m]')
ylabel('u(f) [m/s]')



%Static load plot
plot(x,q_stat)
ylabel('q(z) [Pa]')
xlabel('Height [m]')
```

```
%PRESSURE SPECTER

clear all;

T = 15; %Wind period
U0 = 40; %Mean wind speed
H = 86; %Height above sea level
z = 63; %Mean value used for spectum
rho_a = 1.226; %Air density

%Wind gusts and profile
C = (5.73E-2)*sqrt(1+(0.148*U0));
for i = 1:H
Iu(i) = 0.06*(1+(0.043*U0))*(i/10)^(-0.22);
Uz(i) = U0*(1+(C*log(i/10)));
u(i) = Uz(i)*(1-(0.41*Iu(i)*log(T/3600)));
end

%Static pressure at reference height 46,67 m
q_mean = 0.5*rho_a*Uz(z)^2;

%Frya wind spectrum
n = 0.468;
freq = 0;
for i = 1:60
    f(i) = 172*freq*((z/10)^(2/3))*(U0/10)^(-0.75);
    S = 320*((U0/10)^2)*(z/10)^0.45;
    Sd(i) = S/((1+f(i))^(5/(3*n)));
    freq = freq + 0.1;
    xplot(i) = freq;
    %Pressure spectra
    Sw(i) = ((q_mean^2)*4*Sd(i))/(Uz(z)^2);
end

%Wind speed spectrum plot
plot(xplot,Sd)
xlabel('Frequency [Hz]')
ylabel('Spectral energy density [m^2/s^2Hz] ')

%Wind pressure spectra plot
plot(xplot,Sw)
xlabel('Frequency [Hz]')
ylabel('Spectral energy density [Pa^2/Hz] ')


Swt = Sw';
xplott = xplot';
writefile = 'spec.xlsx';
writefile2 = 'frerange.xlsx';
```

```
xlswrite(writefile,Swt);
xlswrite(writefile2,xplott);

%Reading values from ANSYS
filename = 'freqres2.xlsx';
RAO = xlsread(filename,'B:B');
%Transposed RAO vector
RAOt = RAO';

%Calculating standard deviation
dw = 0.1;
std = 0;
std2 = 0;
omega = 0;
for i = 1:60
    std = std + (Sw(i)*RAOt(i).^2*dw);
    std2 = std2 + ((omega^2)*Sw(i)*RAOt(i).^2*dw);
    omega = omega + 0.1;
end
%Spectral moments
m0 = 0;
m2 = 0;
omega = 0;
for i = 1:60
   m0 = m0 + (Sw(i)*dw);
   m2 = m2 + ((omega^2)*Sw(i)*dw);
   omega = omega + 0.1;
end
```

```
%STRUCTURAL DAMPING
clear all;

%Import frequencies from first m modes
filename = 'eigen.xlsx';
eigen = xlsread(filename,'A:A');
omega = 2*pi*eigen;

m = length(eigen)/2.5;
n = length(eigen);

%Select damping ratios for first and m'th mode
zeta_1 = 0.05;
zeta_m = 0.10;

%Linear interpolation
for i = 1:n
    zeta_lin(i) = (((zeta_m-zeta_1)/(omega(m)-omega(1)))*...
        (omega(i)-omega(1)))+zeta_1;
end

%Linear interpolation of mode 1 < i < m
for i = 1:m
    zeta(i) = (((zeta_m-zeta_1)/(omega(m)-omega(1)))*...
        (omega(i)-omega(1)))+zeta_1;
end

%Extrapolation of values greater than m
for i = m+1:25
    zeta(i) = (((zeta_m-zeta_1)/(omega(m)-omega(1)))*...
        (omega(i)-omega(m)))+zeta_1;
end

%Obtaining beta value based on first data set
beta = ((2*zeta_1*omega(1))-(2*zeta_m*omega(m)))/...
    (omega(1)^2-omega(m)^2);

%Back-subsituting beta and obtaining alpha value
alpha = (2*zeta_1*omega(1))-(beta*omega(1)^2);

%Calculating beta value based on second data set
beta2 = ((2*zeta_1*omega(1))-(2*zeta(n)*omega(n)))/...
    (omega(1)^2-omega(n)^2);

%Alpha value based on second data set
alpha2 = (2*zeta_1*omega(1))-(beta2*omega(1)^2);

%Alpha and beta based on average values of the two first data sets
zeta_avg = (zeta_m+zeta(n))/2;
```

```
omega_avg = (omega(m)+omega(n))/2;

beta_avg = ((2*zeta_1*omega(1))-(2*zeta(n)*omega_avg))/...
    (omega(1)^2-omega_avg^2);
alpha_avg = (2*zeta_1*omega(1))-(beta_avg*omega(1)^2);

%Damping ratio for the 3 different sets of alpha and beta
for i = 1:n
    lambda1(i) = 0.5*((alpha/omega(i))+beta*omega(i));
    lambda2(i) = 0.5*((alpha2/omega(i))+beta2*omega(i));
    lambda_avg(i) = 0.5*((alpha_avg/omega(i))+beta_avg*omega(i));
end

plot(omega,zeta_lin,omega,lambda1,omega,lambda2,omega,lambda_avg)
xlabel('omega [rad/s]')
ylabel('lambda [-]')
legend('Linear interpolation','First 10 modes','Full range',...
    'Average values','Location','NorthWest')

%Calculating deviations
dev1 = 0;
dev2 = 0;
dev_avg = 0;
for i = 1:n
    dev1 = dev1 + abs(zeta_lin(i)-lambda1(i));
    dev2 = dev2 + abs(zeta_lin(i)-lambda2(i));
    dev_avg = dev_avg + abs(zeta_lin(i)-lambda_avg(i));
end

%Determinate damping approximation closest to the linear interpolation
if dev1 < dev2 && dev1 < dev_avg
    beta_a = beta;
    alpha_a = alpha;
elseif dev2 < dev_avg
    beta_a = beta2;
    alpha_a = alpha2;
else
    beta_a = beta_avg;
    alpha_a = alpha_avg;
end

%Write alpha and beta values
values = [alpha_a,beta_a];
writefile = 'damp.xlsx';
xlswrite(writefile,values);
```

```
%VORTEX INDUCED VIBRATIONS

clear all;

U0 = 40;              %Mean wind speed
L = 70;               %Height of tower
t1 = 0.038;           %Bottom shell thickness
t2 = 0.011;           %Mid shell thickness
t3 = 0.008;           %Top shell thickness
T = 15;               %Mean period
C_a =0.6;             %Added mass coeff.
rho_a = 1.226;        %Density air
rho_s = 7850;         %Density steel
upsilon = 1.5*10^-5;%Kinematic viscosity air
D_mean = 4;           %Mean diameter

%Reading damping coeff., eigenvalues and dimensions from spreadsheet
filename = 'damp.xlsx';
damp = xlsread(filename);
filename2 = 'eigen2.xlsx';
eigen = xlsread(filename2);
filename3 = 'dim.xlsx';
H = xlsread(filename3,'A:A');
D = xlsread(filename3,'B:B');

%Cross sectional areas
for i = 1:6
A(i) = pi*((D(i)/2)^2-((D(i)/2)-t1)^2);
end
for i = 7:12
A(i) = pi*((D(i)/2)^2-((D(i)/2)-t2)^2);
end
for i = 13:19
A(i) = pi*((D(i)/2)^2-((D(i)/2)-t3)^2);
end
Sa = 0;
Sd = 0;
n = length(A);
for i = 1:length(A)
    Sa = Sa + A(i);
    Sd = Sd + D(i);
end

%Equivalent mass
m = (Sa/length(A))*rho_s;
m_a = C_a*pi*(Sd/length(D))^2*rho_a;
m_e = m+m_a;

%Wind profile
```

```
C = (5.73E-2)*sqrt(1+(0.148*U0));
for i = 1:length(H)
Iu(i) = 0.06*(1+(0.043*U0))*(H(i)/10)^(-0.22);
Uz(i) = U0*(1+(C*log(H(i)/10)));
u(i) = Uz(i)*(1-(0.41*Iu(i)*log(T/3600)));
end



alpha = damp(1);
beta = damp(2);
%Damping ratios and stability parameter
for i = 1:length(eigen)
    zeta(i) = 0.5*((alpha/eigen(i))+(beta*eigen(i)^2));
    delta(i) = 2*pi*zeta(i);
    K_s(i) = (2*m_e*delta(i))/(rho_a*(Sd/length(D))^2);
end

%Reynolds number
for i = 1:length(D)
    Re(i) = u(i)*D(i)/upsilon;
end
St = 0.34;
%Bondaries lock-in
LowerIL = 0.3/St;
UpperIL = 0.65/St;
LowerCF = 0.8/St;
UpperCF = 1.6/St;

%Reduced velocity
for i = 1:length(eigen)
    for j = 1:length(D)
        U_R(i,j) = u(j)/(eigen(i)*D(j));
    end
end

%Mode shapes
n = [1 3 5 7 9 11];
for i = 1:length(eigen)
    sfun1(i) = 0;
    sfun2(i) = 0;
    for j = 1:L-1
        mode(i,j) = sin((n(i)*pi/2)*(j/L))/sin(n(i)*pi/2);
        sfun1(i) = sfun1(i)+mode(i,j).^2;
        sfun2(i) = sfun2(i)+mode(i,j).^4;
    end
end

ymax = max(mode,[],2);
```

```
%Calculating mode shape parameter
for i = 1:length(eigen)
    gamma(i) = ymax(i)*sqrt(sfun1(i)/sfun2(i));
end

%Cross-flow amplitude
for i = 1:length(eigen)
    A_cf(i) = 0.31*gamma(i)*D_mean/sqrt(0.062+0.077*K_s(i)^2);
end
```

```
%DYNAMIC SCATTER
clear all;
%Reading values from ANSYS
filename = 'dynval.xlsx';
dynstress = xlsread(filename,'B:B');

dynstress = dynstress*10^-6;

mode = 0;
for i = 1:25
   mode(i) = i;
end


scatter(mode,dynstress,10);
xlabel('Mode number')
ylabel('Maximum Von Mises Stress [MPa]')
```